International Journal of Mechanical Sciences 314 (2026) 111403

Contents lists available at ScienceDirect

International Journal of Mechanical Sciences

journal homepage: www.elsevier.com/locate/ijmecsci

NCS-BEMNet: A boundary-element-based neural coefficient solver for acoustics

Huilan Wu, Yijun Liu *

Department of Mechanics and Aerospace Engineering, Southern University of Science and Technology, Shenzhen, 518055, Guangdong, China

ARTICLE INFO

Keywords:
Boundary element method
Physics-informed neural networks
Wave equation
Plane-wave expansion
Neural coefficient solver
Global analytic approximation

ABSTRACT

The Boundary Element Method (BEM) and machine learning offer physically rigorous and scalable frameworks for solving wave-based problems, yet traditional approaches often face limitations such as high computational complexity, stringent requirements for boundary smoothness, and solution discretization. To overcome these challenges, this study proposes a novel neural coefficient solver framework, termed NCS-BEMNet, which departs fundamentally from existing neural BEM approaches. Instead of predicting field values or boundary quantities, NCS-BEMNet learns the coefficient mapping of an analytical plane-wave spectral representation, embedding the intrinsic solution structure of the Helmholtz equation directly into the network architecture. This enables an explicit analytical approximation of the acoustic field rather than a purely data-driven surrogate. Distinct from conventional neural solvers, NCS-BEMNet requires no boundary discretization, no special input encoding, and no matrix inversion. Its training loss is strictly constrained by the Boundary Integral Equation, enforcing strong global physical consistency and yielding a continuous solution across the entire domain. By combining analytical solution expressions with neural coefficient learning, the proposed framework preserves the physical characteristics of wave propagation while achieving high computational efficiency. Numerical results demonstrate that NCS-BEMNet maintains accuracy comparable to classical BEM even in complex and large-scale acoustic scattering problems, while significantly outperforming existing BEM-based neural networks in terms of convergence speed and stability.. Numerical results demonstrate that NCS-BEMNet maintains accuracy comparable to classical BEM even in complex and large-scale acoustic scattering problems, while significantly outperforming existing BEM-based neural networks in terms of convergence speed and stability. NCS-BEMNet provides a neural solving paradigm based on analytical solution expressions, laying an important foundation for next-generation intelligent computational methods in wave-based engineering analysis and acoustic simulation.

1. Introduction

Numerical modeling of acoustic phenomena, such as radiation and scattering [1–3], is vital across many engineering fields. These include aerospace, automotive, and underwater acoustics [4–6]. Accurate and efficient prediction of sound fields is essential for noise control and structural health monitoring [7–9]. For decades, classical numerical methods have been the cornerstone of computational acoustics [10–13]. The finite element method (FEM) is well suited for bounded-domain problems but requires special techniques, such as perfectly matched layers (PML) or infinite elements, to truncate unbounded domains when solving exterior problems. These techniques may introduce artificial reflections and increase computational cost [14–16].

In contrast, the boundary element method (BEM) has emerged as a natural choice for exterior acoustic problems governed by the Helmholtz equation [17–20]. By using the fundamental solution, BEM inherently satisfies the Sommerfeld radiation condition at infinity and requires discretization only on the boundary, reducing the problem dimension by one [21]. However, this advantage comes with high computational cost, as BEM typically produces a dense system of linear equations. The assembly and inversion of the system matrix involve computational complexity from $O(N_c^2)$ to $O(N_c^3)$ for N_c boundary elements, making large-scale problems extremely expensive [22–24]. In addition, the accuracy of the traditional boundary element method is highly sensitive to the quality of boundary discretization and the evaluation of singular integrals, often requiring smooth boundaries and complex integration schemes. Moreover, its solution is inherently discrete, defined only at collocation points or within boundary elements, making it difficult to

* Corresponding author.
E-mail address: liuyj3@sustech.edu.cn (Y. Liu).

https://doi.org/10.1016/j.ijmecsci.2026.111403
Received 13 November 2025; Received in revised form 31 January 2026; Accepted 13 February 2026
Available online 14 February 2026

obtain a continuous field representation.

The recent rise of scientific machine learning, especially Physics-Informed Neural Networks (PINNs) [25–29] and Neural Operators [30–33], has provided a promising new paradigm for solving partial differential equations (PDEs) [34,35]. These methods aim to learn solution operators from data or physical laws, potentially avoiding the expensive process of mesh generation [36–38]. The core idea is to incorporate known physical equations and initial or boundary conditions as constraints during neural network training. By embedding these physics-based constraints into the loss function, the network learns to satisfy the governing PDEs while fitting any available data. This approach is well suited for handling complex, high-order PDEs with irregular geometries and diverse boundary conditions.

Since its inception, PINNs have been applied to a wide range of problems [39,40], including elliptic [41], parabolic [42,43], and hyperbolic equations [44], as well as time-varying [45–47] and multiscale systems [48,49]. Typical applications span fluid dynamics governed by the Navier–Stokes equations [50,51], heat transfer [52,53], solid mechanics [52,53], electromagnetics [54,55], acoustic problems [56,57], and material design [58,59], among others. PINNs have also been extended to more complex scenarios [60], such as coupled systems [61], inverse problems [62,63], and dual- or multi-domain problems [64–68], where multiple physical fields or governing equations interact across different regions. These studies demonstrate that PINNs offer flexibility in handling heterogeneous physics, irregular geometries, and incomplete data by embedding governing equations, interface conditions, and boundary constraints directly into the training process. As a result, PINNs have gained increasing attention as a general framework for data-driven and physics-constrained modeling of complex dynamical systems.

Despite their flexibility, these neural methods show limitations in acoustic applications. Their performance is highly sensitive to the choice of network architecture, loss function, and training strategy. The optimal setup is usually problem-dependent and may require extensive computation. In addition, the training process often involves solving partial differential equations at each iteration to enforce physical constraints, which leads to longer training times and higher computational costs compared with traditional numerical methods. Significant challenges remain in modeling problems with oscillatory solutions or complex boundaries. The high computational cost of many existing methods further limits their use in practical engineering problems. Training deep neural networks for complex acoustics can be resource-intensive, requiring large amounts of GPU memory and time. Another fundamental challenge in exterior problems is to ensure that the solution strictly satisfies the Sommerfeld radiation condition. Although it can be weakly enforced through a penalty term in the loss function, this does not guarantee full compliance and may result in non-physical reflections in the far field [69,70].

To address this, the integration of machine learning with the Boundary Element Method (BEM) has gradually become an active research direction. Based on the manner of integration, such approaches can be broadly classified into two main categories. The first category is data-driven BEM acceleration and enhancement methods. These approaches typically employ neural networks as efficient surrogate models or accelerators. For instance, deep neural networks are used to learn parametric representations of Green's functions, approximate core components of BEM matrices, or predict preconditioners for specific geometries or parameters, thereby significantly accelerating the matrix assembly and iterative solution process of conventional BEM [71–73]. Additionally, some studies leverage historical simulation data to train neural networks that directly map geometric or physical parameters to boundary solution distributions, enabling rapid prediction and design optimization for specific types of problems [33,74–76]. While such methods can achieve computational acceleration within predefined parameter ranges, they fundamentally rely on high-quality simulation data, with physical consistency entirely guaranteed by the training data. Moreover, they generally lack good generalization capability and struggle to extend to unseen operating conditions.

The second category is the Boundary Integral Neural Network (BINN) framework [77–81]. Unlike the aforementioned data-driven methods, the BINN adopts a hybrid strategy that combines machine learning with the semi-analytical BEM. This approach uses the fundamental solution or Green's function to transform the original PDE into a Boundary Integral Equation (BIE) that involves only unknown boundary quantities. A neural network is then designed and trained to identify these unknown boundary quantities. Since the network output is processed through the exact BIE, it automatically satisfies the original PDE.

BINN integrates the physical completeness of BEM with the approximation capability of neural networks. It reduces the problem dimensionality by one and naturally embeds the boundary conditions into the governing equations. Compared with many traditional neural network methods, BINN automatically incorporates boundary conditions, keeping the focus on satisfying the BIE and reducing the required training data. By replacing differential operators with integral operators, it removes the need for high-order derivatives of the network output and enhances training stability. Because the integral formulation using the fundamental solution is valid for both bounded and unbounded domains, BINN can handle boundary value problems in both cases.

Despite progress in theory and practice, the performance of BINN on wave problems remains limited. A major challenge is that the neural network must directly predict physical fields or their boundary derivatives, which makes it difficult to capture the analytical characteristics of the wave equation accurately. In addition, the highly oscillatory nature of the boundary integral kernels makes it hard for the network to learn globally coherent physical structures, leading to poor generalization and unstable training. As a result, BINN often inherits the scalability limitations of classical methods while losing some accuracy. A key research gap remains: there is still no end-to-end neural approach that can fully exploit the physical advantages of the boundary integral formulation while overcoming the computational bottlenecks of neural networks.

To address this issue, this paper introduces a neural coefficient solver framework based on the BEM. It aims to achieve high-accuracy and continuously analytic approximations for wave problems. Our main contributions are fivefold:

1. We propose a fundamental shift in which the neural network does not directly approximate the acoustic field. Instead, it learns the optimal coefficients for a basis expansion using plane wave functions, and the solution is then constructed as $p(\mathbf{x}) = \sum_i c_i \psi_i(\mathbf{x})$, where the basis functions $\psi_i(\mathbf{x})$ correspond to plane-wave solutions of the Helmholtz equation. As these functions inherently satisfy the strong-form governing equation, the reconstructed field remains globally consistent with the underlying physics. This formulation naturally enforces the acoustic laws, leading to enhanced stability and spectral accuracy.
2. NCS-BEMNet outputs a continuous analytical function. After training, it can efficiently compute acoustic quantities at any boundary or field point without re-discretization or interpolation, ensuring solution smoothness and physical consistency.
3. Unlike coordinate-based or point-wise learning schemes, NCS-BEMNet does not require explicit spatial inputs, which significantly simplifies the learning procedure and improves training efficiency.
4. The proposed method is fully physics-informed and does not rely on labeled training data or precomputed simulation datasets. The learning process is entirely driven by the boundary integral equations and analytical solution structures, ensuring physical consistency by construction.
5. Although our framework is designed for acoustic problems, wave functions are also fundamental solutions in elasticity, electromagnetics, and fluid dynamics. With appropriate basis functions, the

proposed framework can be extended to these domains, making it a highly scalable and general algorithm.

2. Problem setup and theoretical background

2.1. Acoustic boundary integral equations

The scattering behavior of acoustic surfaces usually involves complex local resonance effects and far-field wave propagation. It represents a typical unbounded-domain acoustic scattering problem. When dealing with surface scattering, traditional methods such as the FEM and the finite difference method (FDM) can provide accurate solutions. However, they require discretization of the entire computational domain and the introduction of absorbing boundary layers, such as PML, to simulate the unbounded condition. This leads to high computational costs, which become particularly significant in multiscale structural analyses.

In contrast, the BEM requires solving only on the structure boundary. It naturally satisfies the unbounded radiation condition and significantly reduces the number of degrees of freedom. For example, in two-dimensional acoustic problems, the boundary integral method only needs discretization along the one-dimensional boundary, while in three dimensions, it only needs to handle the two-dimensional surface boundary. The basic idea is to transform partial differential equations such as the Helmholtz equation into integral equations defined on the boundary. Therefore, our neural operator is trained based on boundary data from the surface. For clarity, a brief introduction to the boundary element method is given below.

The linear acoustic equation in the frequency domain is governed by the Helmholtz equation:

$$\nabla^2\phi + k^2\phi + Q\delta(\boldsymbol{x},\boldsymbol{x}_Q) = 0, \quad \forall \boldsymbol{x} \in D \tag{1}$$

Here, ϕ denotes the complex sound pressure, k is the wavenumber, and Q represents the incident wave. Since the Helmholtz equation is also valid in electromagnetics, the proposed method can be extended to electromagnetic wave analysis. In general, three types of boundary conditions are specified on the boundary S:

$$q \equiv \frac{\partial\phi}{\partial n}; \quad \overline{q} = i\omega\rho v_n; \quad \varphi = Zv_n \tag{2}$$

And it satisfies the radiation conditions at infinity:

$$\lim_{R\to\infty}\left[R\left|\frac{\partial\phi}{\partial R} - ik\phi\right|\right] = 0 \tag{3}$$

here, R denotes the radius of an enclosing sphere surrounding the structure, and ϕ represents the related physical variable. By applying Green's second identity and the properties of the Dirac delta function, Eq. (1) can be transformed into the boundary integral equation (CBIE) form:

$$c(\boldsymbol{x})\phi(\boldsymbol{x}) = \int_S [G(\boldsymbol{x},\boldsymbol{y},\omega)q(\boldsymbol{y}) - F(\boldsymbol{x},\boldsymbol{y},\omega)\phi(\boldsymbol{y})]dS(\boldsymbol{y}) + \phi^I(\boldsymbol{x}) \tag{4}$$

Among them, the Green's function $G(x,y,\omega)$ depends on the dimension of the problem:

$$G(\boldsymbol{x},\boldsymbol{y},\omega) = \begin{cases} \dfrac{i}{4}H_0^{(1)}(kr), & \text{2D} \\ \dfrac{1}{4\pi r}e^{ikr}, & \text{3D} \end{cases} \tag{5}$$

$$F(\boldsymbol{x},\boldsymbol{y},\omega) = \begin{cases} -\dfrac{ik}{4}H_1^{(1)}(kr)r_j n_j(\boldsymbol{y}), & \text{2D} \\ \dfrac{1}{4\pi r^2}(ikr-1)r_j n_j(\boldsymbol{y})e^{ikr}, & \text{3D} \end{cases} \tag{6}$$

Where $r = |\mathbf{x} - \mathbf{y}|$, $\varphi^I(\boldsymbol{x})$ is the incident wave.

$$c(\boldsymbol{x}) = \begin{cases} 1, & \boldsymbol{x} \in D \\ \dfrac{1}{2}, & \boldsymbol{x} \in S(\text{smooth}) \end{cases} \tag{7}$$

under given boundary conditions, Eq. (4) has $c(\boldsymbol{x}) = \frac{1}{2}$ *or* $c(\boldsymbol{x}) = 1$.

In practical applications, once the physical quantities on the boundary are determined, the entire acoustic field, including both near and far fields, can be efficiently obtained through the boundary integral Eq. (4). In the classical BEM, the boundary integral Eq. (4) is discretized by dividing the boundary into a finite number of boundary elements. These elements are used to approximate the boundary geometry and the distribution of physical quantities along it. After discretization, the continuous integral equation is transformed into a dense linear system ($A\phi = b$). Due to the global coupling nature of the Green's kernel, each element interacts with all others, resulting in a computational complexity of $O(N^2)$ for matrix assembly and $O(N^3)$ for direct solution. Therefore, the computational cost of the traditional BEM becomes very high when solving large-scale acoustic scattering problems.

To overcome this problem, we propose a matrix-free framework called NCS-BEMNet. In NCS-BEMNet, the system of equations is neither explicitly constructed nor solved. Instead, the neural network learns the coefficients of plane wave basis functions so that the boundary integral relations are implicitly satisfied. The loss function is defined through boundary integrals, avoiding the explicit assembly and solution of the matrix system.

Developing such a hybrid framework represents a promising and valuable direction in computational acoustics and wave physics. The following section introduces the basic concept of NCS-BEMNet. The fundamental solution of the wave equation can be efficiently represented using a plane-wave spectrum. Specifically, the solution of the wave equation in Eq. (4) can be expressed in wave form, which will be discussed in detail in the next section.

2.2. Two-dimensional acoustic problems

The boundary integral formulation, presented in Eq. (4), makes use of the two-dimensional Green's function in Eq. (5). This Green's function, in turn, is defined by the Weyl (or Sommerfeld) integral, which provides an integral representation for cylindrical waves [82–84]:

$$H_0^{(1)}(kr) = \frac{1}{\pi}\int_0^{\pi} e^{ikr\cos\theta}d\theta \tag{8}$$

Thus, the cylindrical wave solution (Hankel function) to the two-dimensional point source problem can be mathematically constructed from a spectrum of constituent plane waves incident from all directions [85,86]:

$$G(\boldsymbol{x},\boldsymbol{y}) = \frac{i}{4\pi}\int_0^{2\pi} e^{ik(\boldsymbol{x}-\boldsymbol{y})\cdot\hat{\boldsymbol{s}}}d\Omega(\hat{\boldsymbol{s}}) \tag{9}$$

Substituting the result and interchanging the order of integration over the surface s and the angle θ:

$$\phi(\boldsymbol{x}) = \phi^I(\boldsymbol{x}) + \int_0^{\pi}\frac{i}{4\pi}\left[\int_S q(\boldsymbol{y})e^{-ik\hat{\boldsymbol{s}}\cdot\boldsymbol{y}}dS(\boldsymbol{y})\right] - \frac{k}{4\pi}\left[\int_S(\hat{\boldsymbol{s}}\cdot n(\boldsymbol{y}))\phi(\boldsymbol{y})e^{-ik\hat{\boldsymbol{s}}\cdot\boldsymbol{y}}dS(\boldsymbol{y})\right]e^{ik\hat{\boldsymbol{s}}\cdot\boldsymbol{x}}d\theta \tag{10}$$

For numerical implementation, the angular interval $0 \le \theta \le \pi$ is discretized into points θ_m with corresponding weights w_n (e.g., using equi-angular spacing or high-order quadrature rules):

$$\phi(\boldsymbol{x}) \approx \phi^I(\boldsymbol{x}) + \sum_{m=1}^{M} A(\theta_m)e^{ik\hat{\boldsymbol{s}}_m\cdot\boldsymbol{x}}w_m \tag{11}$$

where,

$$A(\theta_m) \approx \frac{1}{4\pi}\left[i\sum_l q(\boldsymbol{y}_l)e^{-ik\hat{\boldsymbol{s}}_m\cdot\boldsymbol{y}_l}\Delta S_l - k\sum_l (\hat{\boldsymbol{s}}_m\cdot\boldsymbol{n}_{y_l})\phi(\boldsymbol{y}_l)e^{-ik\hat{\boldsymbol{s}}_m\cdot\boldsymbol{y}_l}\Delta S_l\right] \tag{12}$$

In the presence of multiple wavenumbers k_n $(n=1,\ldots,N)$ and directions θ_m $(m=1,\ldots,M)$, the analytic approximation is constructed as:

$$\phi(\boldsymbol{x}) \approx \phi^I(\boldsymbol{x}) + \sum_{n=1}^{N}\sum_{m=1}^{M} A_n(\theta_m)e^{ik_n\hat{\mathbf{s}}(\theta_m)\cdot\boldsymbol{x}}w_m \tag{13}$$

This formulation explicitly incorporates information from multiple wavenumbers and directions.

2.3. Three-dimensional acoustic problems

It is well-established that the three-dimensional free-space Green's function also possesses a spectral representation, the Weyl integral. As the derivation closely mirrors that of the two-dimensional problem detailed above, we defer a detailed derivation and present the essential formulation:

$$G(\boldsymbol{x},\boldsymbol{y}) = \frac{ik}{8\pi^2}\int_{S^2} e^{ik\hat{\mathbf{s}}\cdot(\boldsymbol{x}-\boldsymbol{y})}d\Omega(\hat{\mathbf{s}}) \tag{14}$$

The unit sphere s is discretized into M directions $\{\hat{s}_m\}_{m=1}^M$, and the spherical integral is approximated by a quadrature sum with weights w_m:

$$\int_{S^2} f(\hat{s})d\Omega(\hat{s}) \approx \sum_{m=1}^{M} f(\hat{s}_m)w_m \tag{15}$$

The numerical evaluation can be written as:

$$A(\hat{s}_m) \approx \frac{1}{8\pi^2}\left[ik\sum_{l=1}^{L} q(\boldsymbol{y}_l)e^{-ik\hat{\boldsymbol{s}}_m\cdot\boldsymbol{y}_l}\Delta S_l - k^2\sum_{l=1}^{L}(\hat{\boldsymbol{s}}_m\cdot\mathbf{n}(\boldsymbol{y}_l))\phi(\boldsymbol{y}_l)e^{-ik\hat{\boldsymbol{s}}_m\cdot\boldsymbol{y}_l}\Delta S_l\right] \tag{16}$$

By substituting $A(\hat{s}_m)$ back into the summation, a fully discrete plane-wave representation identical to Eq. (20) is obtained. In theory and in practice, the analytical determination of the angular spectrum coefficient $A(\hat{s}_m)$ is extremely difficult. On one hand, $A(\hat{s}_m)$ is nonlocally coupled with the unknown boundary quantities $\phi(y)$ and $q(y)$ through the integral kernel, which causes the coefficient to appear on both sides of the equation and makes explicit separation intractable. On the other hand, for complex boundaries, discretization leads to large-scale, nonsymmetric dense matrices and high-dimensional integral operations, whose computational cost grows exponentially with frequency and geometric scale. Therefore, direct computation of $A(\hat{s}_m)$ is not practical.

To address this problem, this paper proposes a neural coefficient solver. The product of the angular spectrum coefficient and the integral weights is expressed as a complex coefficient vector, and the problem is reformulated as learning a mapping from the boundary field to this coefficient vector, $c = \mathscr{N}_\vartheta(\text{input})$. The detailed framework and implementation are presented in the following section.

3. Methods

3.1. The neural coefficient solver (NCS) framework

As discussed above, the acoustic field can be represented in the frequency domain as a superposition of plane wave bases. Based on Eq. (13), a set of directions $\{\hat{s}_m\}_{m=1}^M$ and the corresponding spherical weights w_m are defined, and the complex coefficients are given by:

$$c_{nm} \triangleq A_n(\hat{s}_m)w_m \in \mathbb{C} \tag{17}$$

The discrete reconstruction of the field is then expressed as:

$$\widehat{\phi}(\boldsymbol{x}) = \phi^I(\boldsymbol{x}) + \sum_{n=1}^{N}\sum_{m=1}^{M} c_{nm}e^{ik\hat{\boldsymbol{s}}_m\cdot\boldsymbol{x}} \tag{18}$$

An extended coefficient set $\widetilde{c}_n$ is defined to include the contribution of the incident wave:

$$\widehat{\phi}(\boldsymbol{x}) = \sum_{n=1}^{N}\sum_{m=1}^{M} \widetilde{c}_{nm}e^{ik_n\hat{\boldsymbol{s}}_m\cdot\boldsymbol{x}} \tag{19}$$

Where $\widetilde{c}_0 = 1$, $\hat{s}_0 = \hat{s}_I$, and $\widetilde{c}_{nm} = c_{nm}$ for $(n=1,\ldots,N; m=1,\ldots,M)$. This formulation provides an analytical approximation of the wave equation under numerical discretization. In theory, when the sampling of wavenumbers and directions is sufficient $(N,M\to\infty)$, the plane wave basis forms a complete set for the Helmholtz equation, allowing the expansion to approximate any physical solution satisfying the radiation condition [87,88]. In the NCS-BEMNet framework, the complex coefficients are given by a neural network:

$$c_{nm} = \mathscr{N}_\vartheta(\mathscr{I}) \tag{20}$$

where, $\mathscr{I}$ represents the available information, such as incident wave amplitude and wavenumber, or even arbitrary random numbers. $\mathscr{N}_\vartheta$ denotes the neural network, where ϑ are the trainable parameters. Thus, the complex nonlinear coefficient-solving problem is transformed into a learnable parameter-mapping process. In implementation, a set of random plane wave basis functions is selected as:

$$\psi_{nm}(\boldsymbol{x}) = e^{ik_n\hat{\boldsymbol{s}}_m\cdot\boldsymbol{x}}, \quad n=1,2,\ldots,N; \quad m=1,\ldots,M \tag{21}$$

where k_n and $\hat{s}_m$ are randomly sampled from given distributions. This construction ensures the analytical continuity and wave-representing capability of the solution. The total field can then be expressed in the neural approximation form as:

$$\widehat{\phi}(\boldsymbol{x}) = \sum_{n=1}^{N}\sum_{m=1}^{M} \widetilde{c}_{nm}\psi_{nm}(\boldsymbol{x}) \tag{22}$$

Hence, the Neural Coefficient Solver converts the original complex, nonlinear coefficient-solving problem into a learnable parameter-mapping problem. This representation enables the network to automatically learn the amplitude and phase of each directional and spectral component, providing a unified representation for both scattering and radiation fields.

Let $\{x_i\}_{i=1}^{N_c}$ be the collocation points on the boundary. The unknown quantities are represented by neural networks $\widehat{\phi}(\boldsymbol{y};\vartheta)$ and $\widehat{q}(\boldsymbol{y};\vartheta) = \frac{\partial\phi(\boldsymbol{y})}{\partial n_y}$, where ϑ denotes the network parameters. The residual of the boundary integral equation at point x_i is defined as:

$$r(\boldsymbol{x}_i;\vartheta) = \int_S \left[\partial_{n_y}G(\boldsymbol{x}_i,\boldsymbol{y};k)\widehat{\phi}(\boldsymbol{y};\vartheta) - G(\boldsymbol{x}_i,\boldsymbol{y};k)\widehat{q}(\boldsymbol{y};\vartheta)\right]dS(\boldsymbol{y}) - \phi^I(\boldsymbol{x}_i) \tag{23}$$

The boundary Γ is parameterized by a local coordinate $\xi\in[-1,1]$, such that $d\Gamma = J(\xi)d\xi$, where $J(\xi)$ is the Jacobian determinant. Boundary integrals are evaluated using Gauss–Legendre quadrature:

$$\int_\Gamma f(\boldsymbol{y})d\Gamma(\boldsymbol{y}) \approx \sum_{l=1}^{N_q} w_l f(\boldsymbol{y}_l)J_l \tag{24}$$

where $\{y_l, w_l, J_l\}$ denote the quadrature points, weights, and Jacobians, respectively, and $N_q$denotes the number of Gauss–Legendre quadrature points Substituting Eq. (21) into Eq. (22) and applying the quadrature rule Eq. (23), the boundary integral residual at a collocation point $x_i\in\Gamma$ is approximated as:

$$r(\boldsymbol{x}_i;\vartheta) = \sum_{l=1}^{N_q} w_l J_l\left[\frac{\partial G(\boldsymbol{x}_i,\boldsymbol{y}_l)}{\partial n_y}\widehat{\phi}(\boldsymbol{y}_l;\vartheta) - G(\boldsymbol{x}_i,\boldsymbol{y}_l)\widehat{q}(\boldsymbol{y}_l;\vartheta)\right] - \phi^I(\boldsymbol{x}_i) \tag{25}$$

The network learns the boundary field representation by minimizing this residual during training. The loss function is defined as the mean squared residual:

$$\widehat{\mathscr{L}}(\vartheta) = \frac{1}{N_c}\sum_{i=1}^{N_c} |r(\boldsymbol{x}_i;\vartheta)|^2 + \lambda \sum_{n=1}^{N}\sum_{m=1}^{M} |\tilde{c}_{nm}|^2 \tag{26}$$

where the second term penalizes excessively large spectral coefficients and λ is a regularization parameter. By minimizing $\widehat{\mathscr{L}}(\vartheta)$, the network automatically learns the boundary field representation that satisfies the boundary integral equation. The predicted spectral coefficients gradually approach the optimal coefficients corresponding to the analytical solution. This process avoids explicit matrix inversion numerically while maintaining analytical continuity and physical completeness.

Fig. 1 is the flowchart of the proposed NCS-BEMNet framework. The model takes as input the global physical parameters, such as the incident wave number k_I and boundary conditions ϕ_I. A deep neural network learns the complex-valued spectral coefficients $\tilde{c}_{nm}$, which represent the weighting factors for the plane-wave basis functions $\psi_{nm}(\boldsymbol{x})$. These coefficients are combined to construct the continuous analytical approximation of the acoustic field $\hat{\phi}(\boldsymbol{x})$. The predicted field is then constrained by the BIE, where the residual $r(\boldsymbol{x}_i;\vartheta)$ is evaluated at selected boundary collocation points. The training objective $\widehat{\mathscr{L}}(\vartheta)$ minimizes the mean squared residual error, enforcing the physical consistency of the solution. The optimizer updates the network parameters iteratively until the residual is minimized, yielding a globally smooth and physically consistent field representation $\hat{\phi}(\boldsymbol{x})$.

3.2. Comparison with vanilla BINN and traditional BEM

To further elucidate the theoretical advantages of the proposed method, this section provides a systematic comparison at the conceptual level between the NCS-BEMNet, the traditional BEM, and the BINN. Although all three methodologies are grounded in boundary integral equation theory and strictly adhere to the governing physical equations (e.g., the Helmholtz equation), they exhibit fundamental differences in solution construction, the mechanism for enforcing physical constraints, and computational framework. The traditional BEM obtains a discrete solution by discretizing the integral kernels and explicitly solving the resulting algebraic system. In contrast, the NCS-BEMNet employs analytical basis functions (such as plane waves) and utilizes a neural network to learn the superposition coefficients, thereby constructing a continuous, analytical-type approximation of the solution. This paradigm represents a shift from numerical discretization to a neuro-analytical representation, endowing the solution process with greater flexibility and scalability while retaining physical rigor (Tables 1–3).

In summary, NCS-BEMNet preserves the physical rigor of the boundary integral formulation while achieving a global analytical approximation of the solution through the learning of plane-wave

Table 1
Core characteristics of the traditional BEM.

Characteristic	Description
Core Principle	A discretization-based numerical method derived from the BIE.
Solution Construction	$\phi(\boldsymbol{x}) = \sum_{j=1}^{N_c}\left[\int_{\Gamma_j} G(\boldsymbol{x},\boldsymbol{y})\,d\Gamma(\boldsymbol{y})\right]q_j - \sum_{j=1}^{N_c}\left[\int_{\Gamma_j}\frac{\partial G(\boldsymbol{x},\boldsymbol{y})}{\partial n_{\boldsymbol{y}}}\,d\Gamma(\boldsymbol{y})\right]\phi_j$
Physical Consistency	Strictly enforced through the discretized form of the integral equation. Numerical errors primarily stem from boundary discretization, element interpolation, and numerical integration accuracy.
Computational Procedure	Mesh discretization → Assembly of coefficient matrices (H, G) → Application of boundary conditions → Solution of the linear system ($\boldsymbol{Ax}=\boldsymbol{b}$) → Post-processing.
Efficiency Analysis	**Computational Complexity:** Matrix assembly $O(N^2)$, direct solution $O(N^3)$. **Advantages:** High accuracy for linear problems in homogeneous media; automatically satisfies far-field radiation conditions. **Disadvantages:** Computational and memory costs scale poorly with problem size.

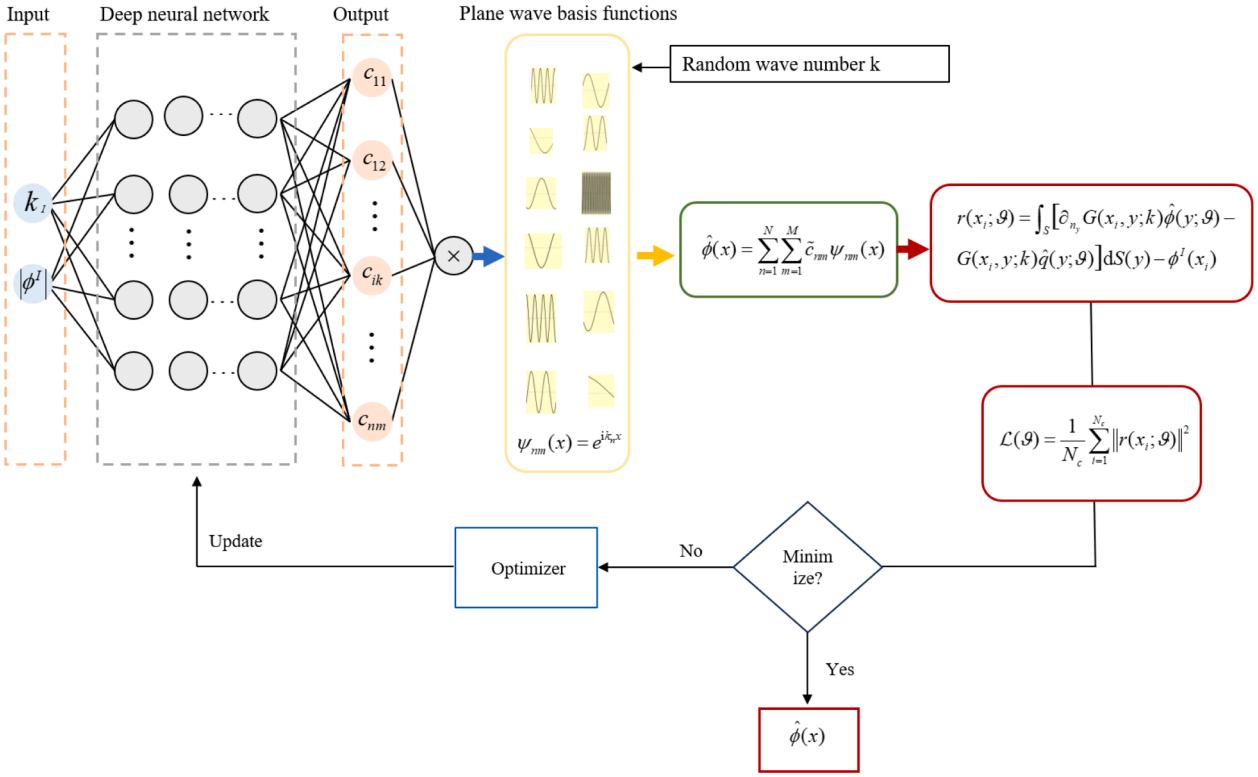

Fig. 1. Overall framework of the proposed NCS-BEMNet.

Table 2
Core characteristics of the BINN.

Characteristic	Description
Core Principle	The unknown physical quantities on the boundary (e.g., potential ϕ and its normal flux q) are parameterized by Deep Neural Networks (DNNs).
Solution Construction	$u(\boldsymbol{y}) \approx \mathrm{NN}_{\phi}(\boldsymbol{y};\Theta_{\phi}), \quad q(\boldsymbol{y}) \approx \mathrm{NN}_{q}(\boldsymbol{y};\Theta_{q})$
Physical Consistency	Enforced via a soft constraint by incorporating the BIE residual into the loss function: $\mathscr{L} = \frac{1}{N_c}\sum_{i=1}^{N_c} \parallel \int_{\Gamma}\left[G(\boldsymbol{x}_i,\boldsymbol{y})q(\boldsymbol{y}) - \frac{\partial G(\boldsymbol{x}_i,\boldsymbol{y})}{\partial n_y}\phi(\boldsymbol{y})\right]d\Gamma(\boldsymbol{y}) \parallel^2$ Accuracy depends on network capacity and the sufficiency of training.
Computational Procedure	Define network architecture → Sample collocation points randomly on the boundary → Compute the boundary integral loss → Optimize network parameters Θ via backpropagation → Inference.
Efficiency Analysis	**Computational Complexity**: No matrix assembly or inversion; per-iteration cost depends on the number of collocation points. **Advantages:** Meshless; continuous solution; well-suited for parametric and inverse problems. **Disadvantages**: Training convergence can be unstable; handling singular integrals requires special techniques; sensitive to network hyperparameters.

spectral coefficients. Compared with the discrete numerical solutions obtained by conventional BEM, the proposed method produces a continuous and differentiable analytical representation, which provides more intuitive physical interpretability and natural advantages for parametric design and inverse optimization. Furthermore, by eliminating the need for explicit matrix assembly and inversion, NCS-BEMNet exhibits improved computational efficiency and stability in large-scale, high-frequency, and geometrically complex problems. This paradigm shift from numerical integration to neural analytical approximation opens a new direction for boundary-integral-based modeling and solution of wave phenomena.

4. Numerical examples

In this section, several numerical results of NCS-BEMNet are presented. The current study primarily focuses on problems governed by the wave equation. The accuracy of the trained model is evaluated by comparing the predicted boundary values with the reference results obtained from the classical BEM. The relative error norm is defined as:

$$E_r = \frac{\sum_{I=1}^{N_c}\left[\widehat{\phi}_I - \phi_{\mathrm{ref}}\right]^2}{\sum_{I=1}^{N_c}\left[\phi_{\mathrm{ref}}\right]^2} \tag{27}$$

where $\widehat{\phi}_I$ denotes the predicted solution, and N_c is the number of boundary points. All numerical experiments were conducted on a Windows workstation equipped with an NVIDIA GeForce RTX 4080 GPU, and the model training was performed using CUDA 12.8.

4.1. Two-dimensional scattering

4.1.1. Accuracy verification

We investigate the performance of NCS-BEMNet on representative problems governed by the wave equation. To verify the accuracy of the model, we first consider a two-dimensional circular scattering problem with rigid boundary conditions, for which an analytical solution is available. The governing equation is given as follows:

$$\begin{cases} \nabla^2\phi(\boldsymbol{x}) + k^2\phi(\boldsymbol{x}) = 0 & \text{in}\mathbb{R}^2\backslash\Omega \\ \dfrac{\partial\phi(\boldsymbol{x})}{\partial n} = 0 & \text{on}\Gamma \\ \lim\limits_{r\to\infty} r^{1/2}\left(\dfrac{\partial\phi_{\mathrm{sc}}}{\partial r} - ik\phi_{\mathrm{sc}}\right) = 0, \quad \phi_{\mathrm{sc}} = \phi - \phi_I \end{cases} \tag{28}$$

where $k = \frac{\omega}{c}$ is the wavenumber, ω is the angular frequency, and c denotes the sound speed.

This system of equations describes the scattered acoustic field $\phi(\boldsymbol{x})$ in an unbounded domain Ω, generated by a prescribed acoustic source $f(\boldsymbol{x})$ acting on the boundary Γ of the scatterer.

For a circular scatterer of radius a with a rigid boundary condition, and an incident plane wave propagating along the x-axis given by $\phi_I(x) = e^{ikx}$, the analytical expression for the total acoustic pressure can be written as follows:

$$\phi(r,\theta) = \sum_{n=-\infty}^{\infty} \epsilon_n i^n\left[J_n(kr) - \frac{J_{n'}(ka)}{H_n^{(1)\prime}(ka)}H_n^{(1)}(kr)\right]e^{in\theta} \tag{29}$$

where, (r,θ) denotes the polar coordinates of the field point. $J_n(\cdot)$ represents the Bessel function of the first kind of order n, and $H_n^{(1)}(\cdot)$ denotes the Hankel function of the first kind of order n. ϵ_n is the Neumann factor, defined as ($\epsilon_0 = 1, \quad \epsilon_n = 2$ for $n \geq 1$). The geometry of the problem is illustrated in Fig. 2(a). A total of 120 collocation points are uniformly distributed along the circular boundary of radius ($r = 1$). The neural network was trained for 4000 iterations, with a total training time of 11.01 s. The evolution of the loss function during training is shown in Fig. 2(b). In this example, the unknown variable $\phi(\boldsymbol{x})$ is defined on the boundary, and the corresponding results are presented in Fig. 2(c) following the point order indicated in Fig. 2(a). It can be observed that the solution obtained by NCS-BEMNet agrees very well with the reference analytical result.

After obtaining the boundary values, the exterior acoustic field is computed using the standard BEM formulation given by Eq. (4). The resulting field distributions are displayed in Figs. 2(d)–(f), where the inset in the upper-right corner shows the boundary solution. The relative L2 error, evaluated using Eq. (32), is $E_r = 5.3 \times 10^{-7}$. When the field point is located very close to the boundary, the standard Gaussian

Table 3
Core characteristics of the NCS-BEMNet.

Characteristic	Description
Core Principle	The neural network does not directly predict field quantities but learns the optimal superposition coefficients for a set of analytical basis functions (e.g., plane waves) that inherently satisfy the governing equation in the domain.
Solution Construction	$\phi(\boldsymbol{x}) \approx \sum_{n=1}^{N}\sum_{m=1}^{M} c_{nm}\psi_{nm}(\boldsymbol{x})$, where the coefficients $c_{nm} = NCS(\vartheta)$. The solution is a continuous, analytical combination of these basis functions.
Physical Consistency	$\mathscr{L} = \frac{1}{N_c}\sum_{i=1}^{N_c} \parallel \int_{\Gamma}\left[G(\boldsymbol{x}_i,\boldsymbol{y})\sum_{n=1}^{N}\sum_{m=1}^{M} c_{nm}\frac{\partial\psi_{nm}(\boldsymbol{x})}{\partial n} - \frac{\partial G(\boldsymbol{x}_i,\boldsymbol{y})}{\partial n_y}\sum_{n=1}^{N}\sum_{m=1}^{M} c_{nm}\psi_{nm}(\boldsymbol{x})\right]\mathrm{d}\Gamma(\boldsymbol{y})\parallel^2$
Computational Procedure	Select basis functions → Construct the coefficient network → Sample boundary points to compute the matrix-free loss → Train the network to learn the mapping $\vartheta \to c_{nm}$ Reconstruct the full-field solution rapidly using the learned coefficients.
Efficiency Analysis	**Computational Complexity:** Combines the matrix-free advantage with the efficiency of learning in a low-dimensional coefficient space, typically leading to faster convergence. **Advantages**: Highest level of physical consistency; no input required; Approximate analytical solution, global approximation. **Disadvantages**: Choice of basis functions is problem-dependent.

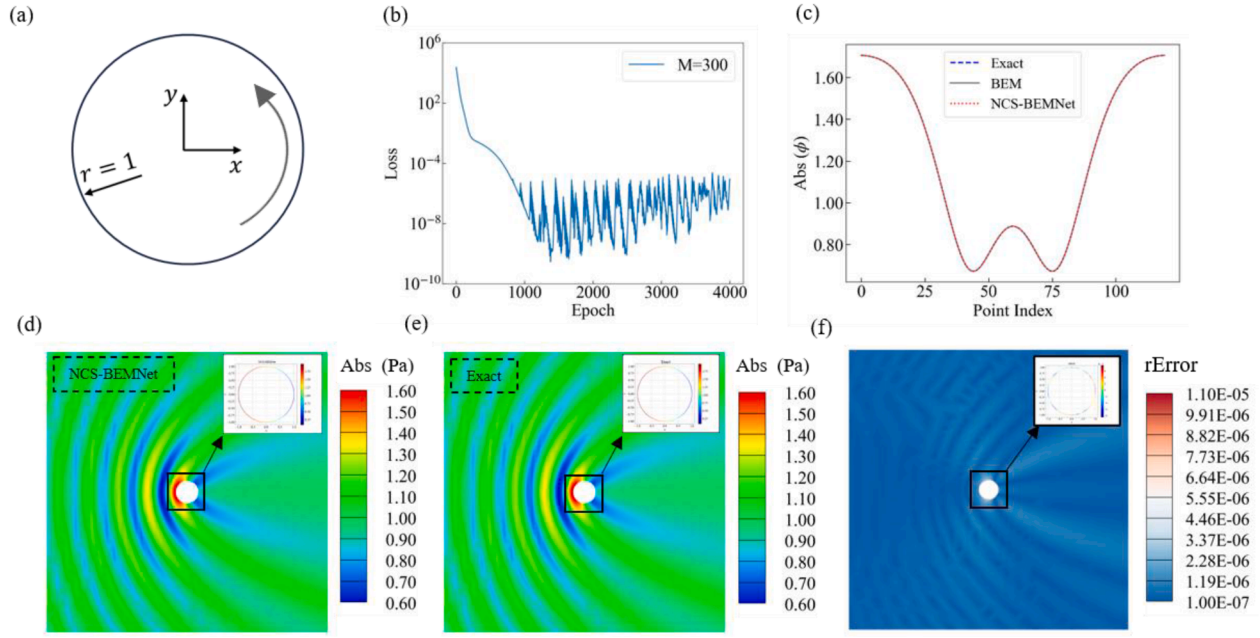

Fig. 2. Computation results of the acoustic scattering field from a rigid circular cylinder under two-dimensional boundary conditions. (a) Geometric configuration of the cylindrical domain; (b) Evolution of the loss function during the training of the cylinder scattering problem; (c) Comparison of the exact solution, conventional BEM solution, and NCS-BEMNet prediction along the boundary; (d) Field distribution of the exact solution; (e) Field distribution obtained by NCS-BEMNet; (f) Relative error distribution of the acoustic field. At this stage, all network parameters are fixed (frozen).

quadrature becomes inaccurate; therefore, a small offset distance of $\varepsilon = 0.02$ is maintained between the field point and the boundary in this example. The results demonstrate that the proposed method achieves highly accurate solutions in unbounded domains. It is worth emphasizing that, at this stage, all network parameters are fixed, allowing rapid evaluation of acoustic quantities at any location on or outside the boundary.

4.1.2. Ablation research

In this section, the effect of various parameters on the training accuracy of NCS-BEMNet is analyzed. The study includes both neural network hyperparameters, such as the number of layers and neurons, and the parameters associated with the analytical basis functions, namely the number of wavenumbers n and the number of propagation directions mmm used in the basis expansion. Here, n denotes the number of distinct wavenumbers k_n, and mmm represents the number of plane-wave directions $\hat{s}_m$ corresponding to each wavenumber. The total number of expansion coefficients is therefore $n \times m$. The number of neurons in each layer is set to 8, 16, and 64, while the network depth is chosen as 1, 2, and 5 layers. For the basis functions, the number of wavenumbers is set to 1, 10, and 100, and the number of propagation directions per wavenumber M is chosen as 50, 100, 120, 150, and 200. In all subsequent ablation studies, the figures present the complete training loss curves plotted on a logarithmic scale. The tables adjacent to each figure list the mean relative errors for the corresponding parameter configurations. For clarity, the variable nk is used in the figures to denote the number of wavenumbers employed in the basis functions.

Although geometric information can be introduced into the training process through boundary mesh nodes, incorporating a large number of nodal data as network inputs remains computationally demanding for large-scale models. This issue will be further discussed in Section 5. In contrast, the proposed NCS-BEMNet trains only the expansion coefficients, which are independent of the geometric configuration. Consequently, the input can be flexibly defined in terms of incident wave parameters, such as wavenumber or amplitude, or even by using a set of randomly sampled data.

Extensive experiments demonstrate that for two-dimensional benchmark problems, an appropriate selection of neural coefficients can yield highly accurate results. As shown in Fig. 3(a), when $M \geq 150$, the training error decreases to 3.02×10^{-4}, whereas insufficient basis sampling $(M < 100)$ leads to noticeable prediction inaccuracies. Since this approach constructs the field solution analytically as a linear combination of coefficients and plane-wave basis functions, the results indicate that at least one hundred coefficients are required to obtain an accurate analytical representation of sound scattering in an unbounded domain. By comparison, classical numerical approaches would need to assemble and solve a system with at least a similar number of equations, even for a simple two-dimensional cylindrical case, resulting in a considerable computational burden for direct solvers.

Fig. 3(b) illustrates the effect of the number of wavenumbers nk on the training loss under a fixed number of propagation directions. It can be observed that as nk increases, the convergence rate of the model slightly improves. When only a single wavenumber $nk = 1$ is used, the loss curve stabilizes after approximately 120 epochs, whereas for nk=2, convergence is achieved after about 100 epochs. However, despite the faster convergence, the final training accuracy shows no significant improvement, indicating that increasing the number of wavenumbers has a limited effect on the model's approximation accuracy.

This behavior is primarily attributed to the completeness of the basis functions. According to the plane-wave expansion theory, any acoustic field that satisfies the Helmholtz equation can be approximated as a linear combination of plane waves propagating in different directions. When the number of directions M is sufficiently large, the basis space becomes nearly complete and can adequately represent the target acoustic field. In other words, the number of directions M governs the spatial coverage of the basis functions and is therefore the dominant factor affecting the accuracy. The number of wavenumbers, by contrast, only contributes limited diversity along the frequency dimension and plays a secondary role in improving the model's representational capacity.

Hence, under constraints of computational or data resources, ensuring a sufficient number of propagation directions should be prioritized to maintain the completeness of the basis space and achieve higher modeling accuracy. It is also noteworthy that when nk=100, the

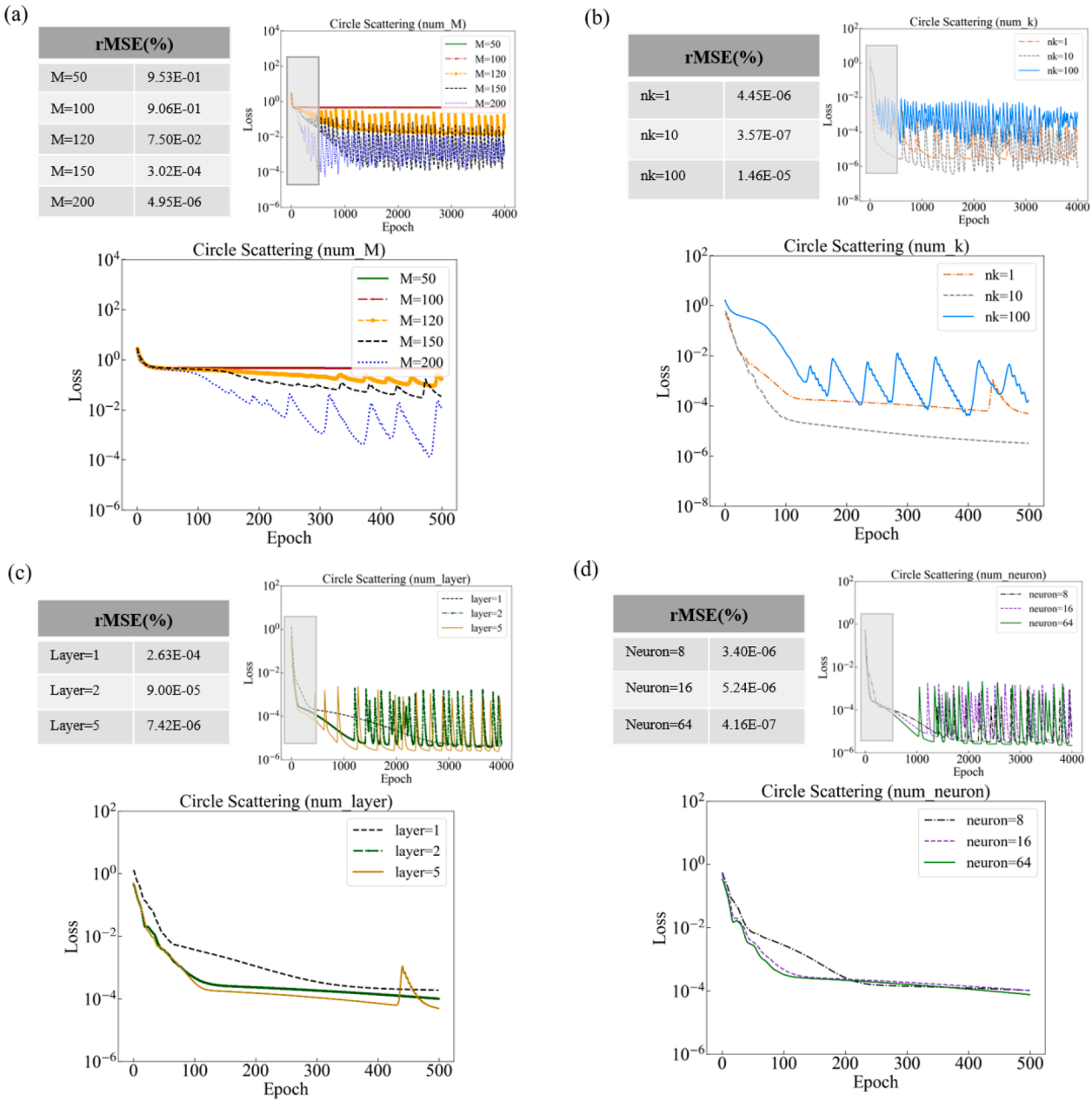

Fig. 3. Training loss convergence under different configurations of plane-wave bases and neural network settings for a two-dimensional scattering problem. For each subfigure, the inset in the upper left corner reports the final relative training error corresponding to the displayed configuration, while the upper right inset shows the full training loss history over all epochs. The bottom panel provides a magnified view of the training loss curves over epochs 0–500 to better illustrate the early-stage convergence behavior. (a) Training loss curves obtained with different numbers of plane-wave basis coefficients M. (b) Training loss curves for different numbers of incident plane-wave directions *n*k. (c) Training loss curves corresponding to different neural network depth (number of hidden layers). (d) Training loss curves obtained using different numbers of neurons per hidden layer.

training accuracy not only fails to improve but even deteriorates. This degradation is caused by spectral confusion in multi-frequency optimization, where discrepancies in the physical behavior of different frequencies lead to conflicting optimization objectives. Meanwhile, the limited network capacity prevents accurate representation of all frequency components within the high-dimensional spectral space. This observation further reveals a fundamental trade-off between frequency extrapolation and dense spectral sampling.

In three-dimensional problems, the complexity of the system increases significantly, and the influence of the wavenumber k on the representational capacity of the acoustic field becomes more pronounced. This is because, in higher-dimensional spaces, the spectral distribution of the wave field is more intricate, and variations in the wavenumber can enrich the frequency components of the basis functions, thereby improving the accuracy of the field approximation. Nevertheless, the number of propagation directions M remains the primary factor determining the completeness of the basis set. It directly controls the spatial density of plane-wave distributions and thus governs the overall accuracy of the acoustic field representation. This trend will be further demonstrated in the three-dimensional numerical examples presented in the following section.

In the NCS-BEMNet framework, increasing the number of neural layers and neurons theoretically enhances the nonlinear representation capability of the model, which may improve training accuracy. However, as shown in Fig. 3(c)(d), when the network depth reaches two layers, the prediction error already decreases to the order of 10^{-5}. With

a single hidden layer, the convergence becomes slightly slower, yet the final accuracy still reaches the order of 10^{-4}. Moreover, further increasing the number of neurons has almost no observable effect on the results. These observations indicate that extending the network depth and width provides only marginal improvement in performance.

This behavior can be explained by the intrinsic formulation of NCS-BEMNet. In this framework, the governing Helmholtz equation is strictly and automatically satisfied through the analytical properties of the plane-wave basis functions, while the boundary conditions are strongly enforced by minimizing the residuals of the boundary integral equation. As a result, the neural network is not required to discover the underlying physical laws. Instead, it searches for the optimal set of coefficients within a solution space that is strictly constrained by the governing physics and defined by the superposition of plane-wave modes. The complexity of this optimization problem is therefore much lower than that of learning the entire physical field from scratch. Consequently, a shallow network with one or two hidden layers, possessing only basic function approximation and optimization capability, is sufficient to achieve high accuracy. The weak sensitivity to the number of neurons further confirms this interpretation, since the dimensionality of the solution space is primarily determined by the number of plane-wave bases M and the discrete wavenumbers , rather than by the internal structure of the neural network. This observation demonstrates that the accuracy and efficiency of the proposed method are governed mainly by the underlying physical formulation, rather than by the size of the neural architecture.

4.2. Three-dimensional scattering

As discussed earlier, NCS-BEMNet can be conveniently applied to unbounded-domain problems. Such problems are common in practical scenarios, including large-scale sonar scattering, as well as acoustic scattering from ultra-thin rotating blade edges. For PINN and conventional BINN approaches, these problems are difficult to handle because the acoustic field extends over an infinite domain and the solution strongly depends on boundary conditions, which require a large number of collocation points. More importantly, the solutions obtained from these black-box networks satisfy the loss constraints of the governing equations but lack explicit physical enforcement during training. As a result, they may produce numerically acceptable yet physically inconsistent results, leading to low accuracy or even failure when solving large or complex problems.

NCS-BEMNet fundamentally overcomes these difficulties. Its solution components strictly satisfy the analytical form of the wave equation, ensuring physical self-consistency and reliability. This property enables accurate and efficient treatment of unbounded-domain problems and provides a new computational paradigm that combines mathematical rigor with practical efficiency for engineering applications.

The effectiveness of the proposed method is validated through four numerical examples with increasing complexity. First, a three-dimensional spherical scattering problem with an analytical solution is used to verify the basic accuracy of the model. Second, the method is applied to a rotating blade with an ultra-thin edge. Finally, the method is applied to a large-scale sonar problem representing a realistic engineering scenario.

4.2.1. Accuracy verification

In this study, a three-dimensional acoustic scattering problem of a rigid sphere is investigated. The model configuration is shown in Fig. 4. The sphere has a radius of 1, and the background acoustic field is a plane incident wave. The analytical solution for the total acoustic field resulting from the scattering is given by:

$$\phi(r,\theta) = \phi_I \sum_{n=0}^{\infty} i^n (2n+1) \left[J_n(kr) - \frac{J'_n(ka)}{H_n^{(1)\prime}(ka)} H_n^{(1)}(kr) \right] P_n(\cos\theta) \tag{30}$$

here,$J_n$denotes the spherical Bessel function of the first kind, and P_n represents the Legendre polynomial. A total of 1200 nodes are distributed along the boundary. The network is trained for 4000 iterations, with a total computation time of 25.47 s. The comparisons among NCS-BEMNet, BEM, and the analytical solution, as well as the corresponding

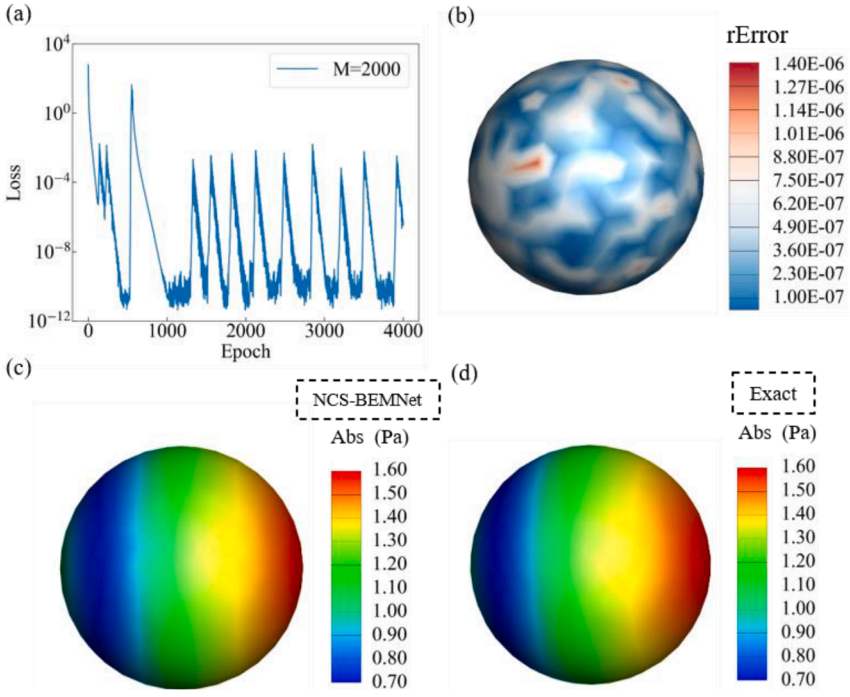

Fig. 4. Results for the three-dimensional spherical scattering problem. (a) Loss curves for the three-dimensional spherical scattering problem. (b) Error distribution between the NCS-BEMNet predicted boundary values and the analytical solution. (c) Boundary values computed by NCS-BEMNet. (d) Boundary values obtained from the analytical solution.

error distributions, are shown in Figs. 4(b) and 4(c)(d). The results indicate that both numerical methods can accurately reproduce the analytical solution. The classical BEM is employed as a reference because, for most complex problems, analytical solutions are unavailable, and validated numerical methods must be used for comparison. Therefore, it is necessary to first verify the accuracy of BEM in this benchmark case. The results in Fig. 4 confirm that the BEM solution is sufficiently accurate to serve as a reliable reference, establishing a solid verification framework for subsequent studies.

Once the boundary values are obtained, the acoustic field at any exterior point can be computed using the corresponding boundary integral formulation, as shown in Fig. 5. The field points are located at a distance of 0.01 from the boundary. The results demonstrate that the proposed method yields highly accurate predictions at the field points, in some cases even surpassing those obtained by the conventional BEM. This improvement arises because the residual error on the boundary oscillates around zero, and these local errors tend to cancel each other when integrated over the boundary, leading to enhanced accuracy in the field evaluation.

Another contributing factor is the analytical structure of the proposed solution. The field is represented as a finite superposition of plane-wave basis functions, which form a complete set in the solution space of the Helmholtz equation. This theoretical completeness ensures that any physically admissible acoustic field can be accurately represented by such an expansion. The approximation error in the present method originates only from the finite number of basis functions and from the network's coefficient approximation, both of which can be effectively reduced through systematic optimization of the network architecture and training parameters.

Unlike conventional numerical methods that yield discrete nodal values, the proposed approach produces a continuous analytical representation of the solution. This representation enables a smooth and physically consistent approximation of the boundary field in the vicinity of the collocation points and across the boundary as a whole. Once the network is trained, high-accuracy predictions at arbitrary boundary or field locations can be obtained directly without additional interpolation or post-processing, thereby overcoming the inherent limitations of classical discrete schemes in terms of flexibility and global consistency.

4.2.2. Ablation studies

As the geometric complexity increases, the training of neural networks generally becomes more challenging. To evaluate the reliability of the proposed model in three-dimensional configurations, corresponding ablation studies were conducted, and the results are shown in Fig. 6. Consistent with the two-dimensional case, the number of neural coefficients M remains the dominant factor influencing model accuracy. This overall trend holds in three dimensions as well. Although the influence of the wavenumber parameter nk is more pronounced in 3D than in 2D, its effect remains marginal; beyond nk=4, the accuracy even decreases, suggesting that excessively large values are not desirable and may increase computational cost without improving performance. The underlying reason is that, as the geometric complexity grows, the acoustic field exhibits richer directional components in space. Increasing the number of directions M enhances the completeness of the basis function space and improves the model's approximation capability, whereas the wavenumber nk mainly introduces frequency diversity, whose contribution is limited and tends to saturate.

As shown in Fig. 6(a and b), the number of boundary points on the three-dimensional sphere is approximately six times that of the two-dimensional cylinder. To achieve the desired accuracy, about $M = 800$ neural coefficients and nk=3 wavenumbers are required. It is expected that as the geometric complexity further increases, both M and nk, particularly M will continue to grow. In conventional numerical methods, achieving a plane-wave expansion of comparable accuracy would require solving a system of equations whose size scales proportionally with $M \times nk$, which is often computationally prohibitive. In contrast, such data volumes are easily handled by neural networks, which can substantially improve model accuracy within an acceptable training time. From the perspective of data scalability and computational efficiency, the proposed method therefore remains effective and extensible for complex geometries.

Fig. 6(c and d) presents the training loss curves under different numbers of neural layers and neurons. When the network depth is one layer, the loss decreases rapidly at the early stage but increases noticeably in the later phase. This behavior indicates that a single-layer network lacks sufficient representational capacity to capture the complex nonlinear relationships among variables, leading to an underfitting condition. When the depth increases to two layers, the training loss stably converges to the order of 10^{-10}, and the curve remains smooth without evident oscillations. This suggests that a two-layer configuration provides adequate depth to represent the essential features of the problem and achieves a balanced fitting performance. However, when the depth is further increased to five layers, the loss initially converges faster to the order of 10^{-9} but rises again in the later stage. This trend implies that an excessively deep network introduces an overfitting tendency, where the model begins to learn noise components in the training data rather than the underlying physical patterns.

Similarly, the variation in the number of neurons exhibits a

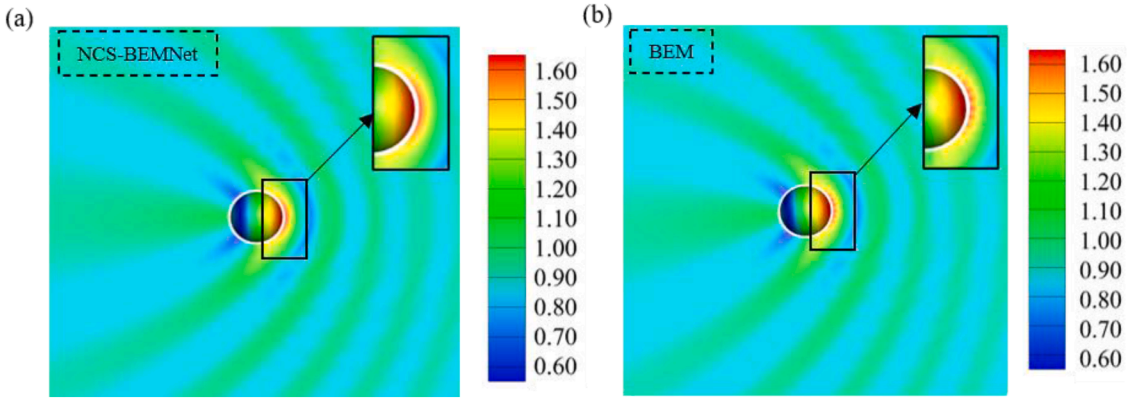

Fig. 5. Comparison of the acoustic pressure magnitude in a three-dimensional rigid sphere scattering problem computed using the proposed NCS-BEMNet and the conventional boundary element method (BEM). The scattered acoustic field is obtained from the boundary solution obtained in Fig. 5. For both methods, the field is evaluated at identical spatial locations in the exterior domain. The inset in the upper right corner of each subfigure shows an enlarged view of the acoustic pressure magnitude in the near-boundary region, highlighting the analytical continuity of the NCS-BEMNet solution in contrast to the piecewise-discrete nature of the conventional BEM solution. (a) Magnitude of the acoustic field computed by NCS-BEMNet. (b) Magnitude of the acoustic pressure field obtained from the conventional BEM.

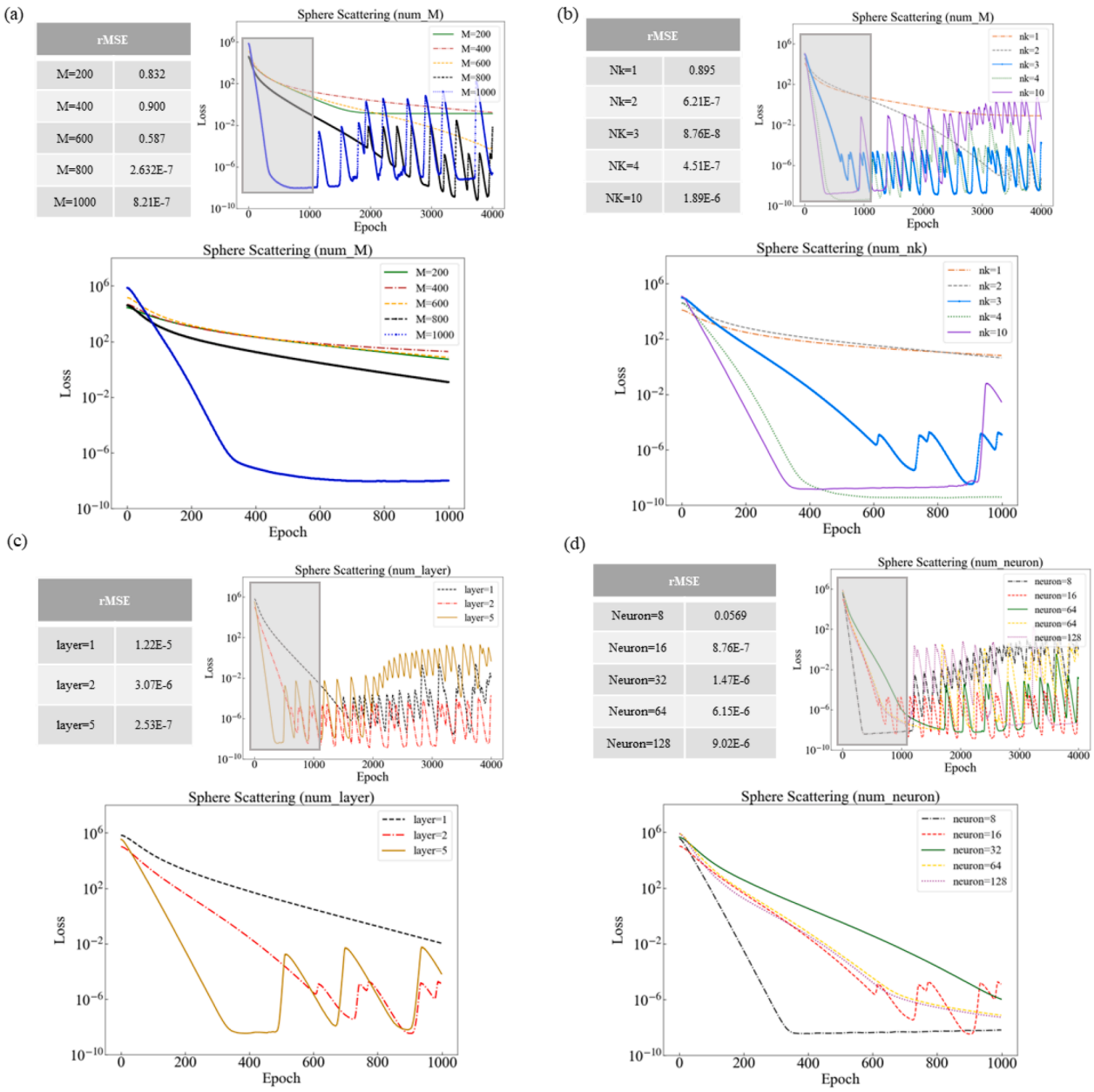

Fig. 6. Training loss convergence under different configurations of plane-wave bases and neural network settings for a three-dimensional scattering problem. For each subfigure, the inset in the upper left corner reports the final relative training error corresponding to the displayed configuration, while the upper right inset shows the full training loss history over all epochs. The bottom panel provides a magnified view of the training loss curves over epochs 0–500 to better illustrate the early-stage convergence behavior. (a) Training loss curves obtained with different numbers of plane-wave basis coefficients M; (b) training loss curves for different numbers of incident plane-wave directions *n*k; (c) training loss curves corresponding to different neural network depth (number of hidden layers); (d) training loss curves obtained using different numbers of neurons per hidden layer.

consistent trend. When the neuron number is set to eight, the loss decreases most rapidly in the early training stage but rises again in the later phase, indicating that the network capacity is insufficient to stably approximate the target function. As the number of neurons increases to between 16 and 32, the loss curve becomes smoother and the convergence more stable, suggesting that the model achieves a better balance between representational power and generalization. However, further increasing the number of neurons causes the loss to rise at later stages, reflecting an overfitting tendency.

The learning process of NCS-BEMNet is guided by the governing physical constraints, where the primary task of the network is to adjust the coefficients and mappings embedded in the physical formulation rather than to perform pure data fitting through deep architectures. When the network is too shallow or narrow, its representation capacity becomes inadequate to capture the complex boundary responses. Conversely, an excessively deep or wide structure introduces too many degrees of freedom, which may deviate from the physical constraints and lead to overfitting or unstable training. Therefore, a moderate network depth of two layers with 16–32 neurons provide an optimal balance among accuracy, stability, and physical consistency.

4.2.3. Scattering problem of three-dimensional propeller

In the study of aircraft and marine noise, the propeller is regarded as one of the primary noise sources. During operation, propellers generate strong unsteady aerodynamic noise. As these acoustic waves radiate outward, they interact with nearby structures such as wings, fuselage

surfaces, or hull components, leading to complex scattering and interference phenomena. Such noise has been identified as a significant source of environmental pollution.

On the other hand, structural components such as wings can be strategically utilized as physical barriers between the propeller noise source and the ground, producing an acoustic shielding effect. This can reduce the overall intensity of the engine and propeller radiated noise while altering its spatial directivity and radiation characteristics.

In this study, we focus on the acoustic scattering effects induced by propellers and employ the NCS-BEMNet method for modeling and analysis. The proposed approach accurately estimates the acoustic field distribution and propagation characteristics of propeller noise sources in complex environments. These capabilities are essential for gaining deeper insight into the generation mechanisms of propeller noise and for guiding the optimization of acoustic control strategies.

As discussed above, NCS-BEMNet can be conveniently applied to exterior problems, that is, problems defined in infinite or semi-infinite domains. Such problems are common in engineering practice. However, conventional machine learning approaches often face difficulties in these cases because the extremely thin boundary region tends to cause inaccurate predictions.

The numerical model is illustrated in Fig. 7. The propeller has a radius of 5 m, and the background pressure field is a plane wave with a unit amplitude, a total of 8956 boundary nodes are defined. The network is trained for 6000 iterations. Fig. 7 presents the error distributions of the NCS-BEMNet solution in comparison with the classical BEM solution and the commercial software COMSOL. Fig. 7(a) shows the training loss curve, Figs. 7(b) and 7(c) display the relative error distributions with respect to BEM and COMSOL, respectively, and Figs. 7(d)–7(f) provide a detailed comparison of the results obtained by the three methods. The results indicate that the NCS-BEMNet solution is in close agreement with both BEM and COMSOL, with low relative errors observed across the computational domain.

After obtaining the numerical solutions of all boundary variables, the acoustic quantities at arbitrary field points outside the domain can be computed using Eq. (4). For complex geometries such as propellers, the boundary region usually corresponds to the area where the acoustic quantities reach their maximum values, and thus represents the most critical part in both analysis and engineering design. Therefore, this section primarily presents the computational results on the boundary.

The results show that the error distribution is relatively uniform, and the overall prediction accuracy is high. The relative error generally remains on the order of 10^{-5}, with the maximum value of approximately 0.015 observed only at a few isolated points. These local deviations mainly arise from stochastic factors during neural network training, such as random parameter initialization and batch sampling variations. Performing multiple independent training runs and averaging the results can effectively reduce the influence of such random errors, thereby further improving the stability and overall accuracy of the predictions.

4.2.4. *Sound scattering of large-scale sonar models*

In this section, the NCS-BEMNet method is applied to the acoustic analysis of a large sonar platform with an overall length of approximately 80 m. The model exhibits typical large-scale and geometrically complex boundary characteristics, representative of underwater vehicles or acoustic detection systems in practical engineering applications. Evaluating the performance of NCS-BEMNet on such a configuration allows assessment of its modeling capability and predictive accuracy in large-scale and strongly nonuniform acoustic fields. This study holds both theoretical and engineering significance for advancing the acoustic stealth design and noise control of large underwater structures.

As shown in Fig. 8, the boundary of the platform model contains 12,788 nodes. The results demonstrate that NCS-BEMNet achieves very high accuracy in computing the acoustic field in unbounded domains, with most of the residual errors concentrated near the boundary. This behavior arises because the acoustic quantities on the boundary are fully predicted by NCS-BEMNet, and the remaining discrepancies primarily originate from the network's approximation of boundary responses. However, when these predicted boundary quantities are subsequently used in the boundary integral formulation to evaluate the exterior acoustic field, part of the boundary prediction errors is counterbalanced by the integration process. As a result, the predicted far-field pressure

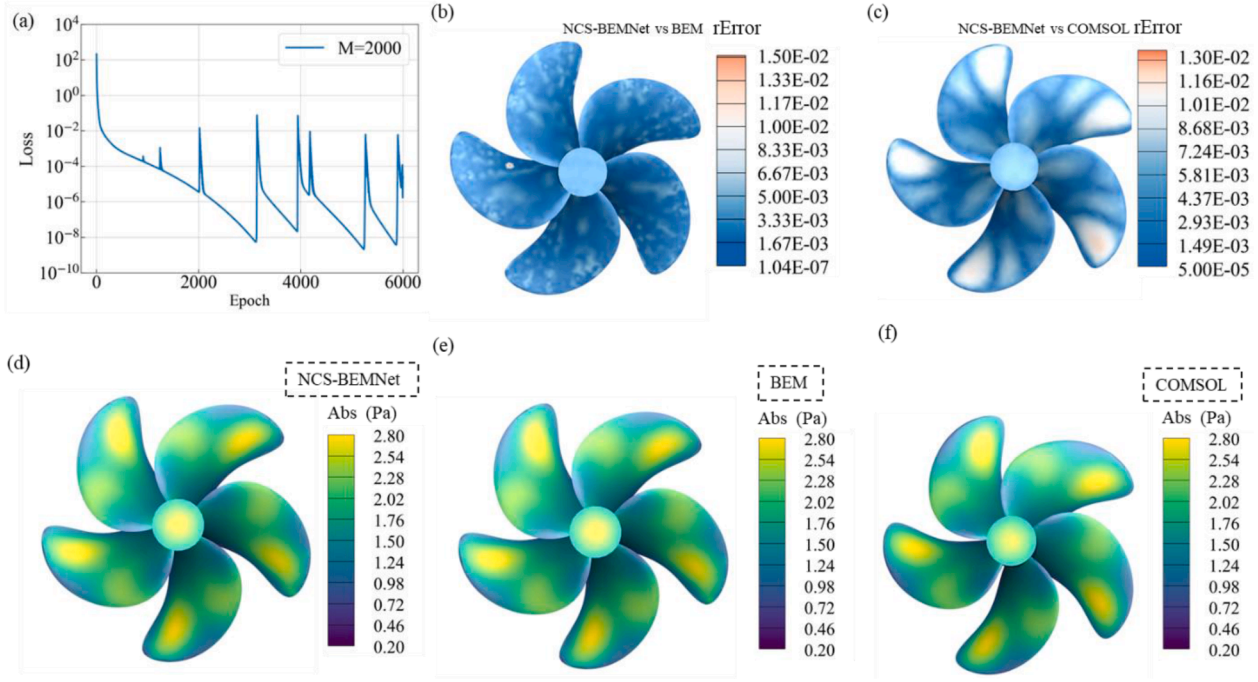

Fig. 7. Comparison of NCS-BEMNet predictions with conventional BEM and COMSOL for propeller scattering problem. (a) Training loss curve for the propeller scattering problem; (b) Distribution of the relative error obtained by NCS-BEMNet vs BEM. (c) Distribution of the relative error obtained by NCS-BEMNet vs COMSOL. (d) Computed result obtained by NCS-BEMNet. (e) Computed result obtained by the conventional BEM. (f) The reference solution obtained from COMSOL.

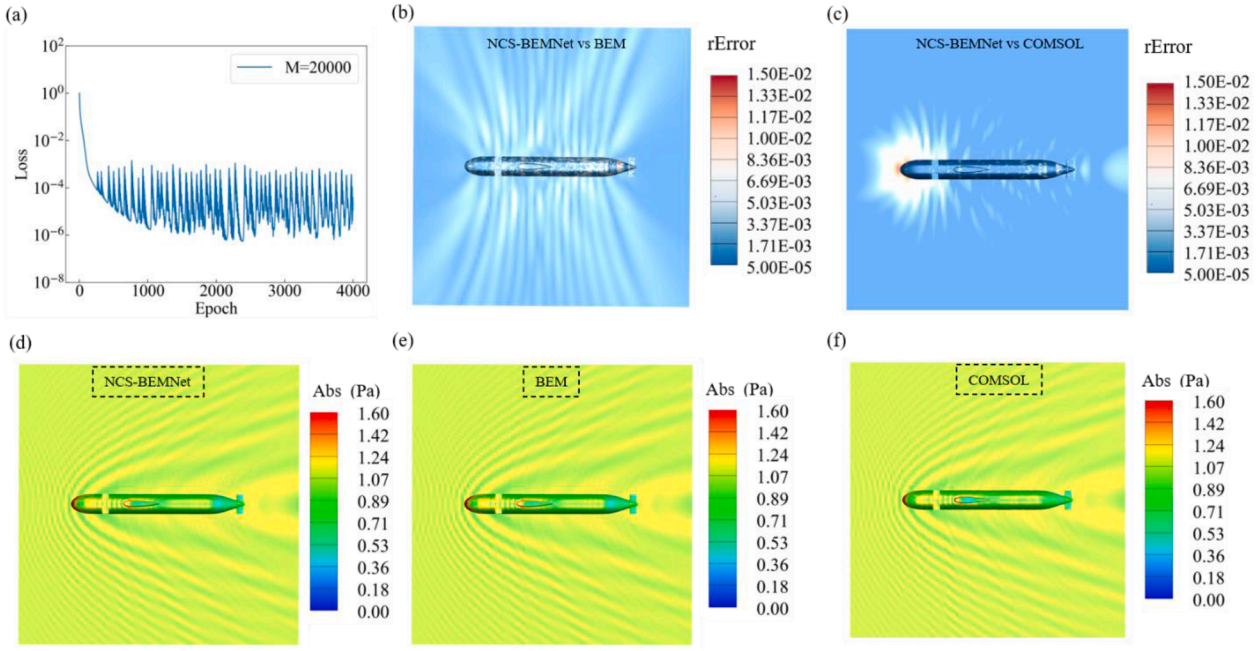

Fig. 8. Performance comparison of the proposed NCS-BEMNet with conventional numerical solvers for a large-scale sonar acoustic scattering problem. (a) Loss curve computed by NCS-BEMNet. (b) Relative error of the NCS-BEMNet results with respect to the BEM solution. (c) Relative error of the NCS-BEMNet results with respect to the COMSOL solution. (d) Acoustic field predicted by NCS-BEMNet. (e) Acoustic field obtained from the conventional BEM. (f) Acoustic field obtained from the COMSOL.

distribution becomes even more accurate than the direct boundary estimates.

This observation indicates that, when coupled with the BIE, NCS-BEMNet benefits from the intrinsic physical consistency of the integral representation. The integration process introduces a self-correcting mechanism for the learned boundary errors, thereby enhancing the stability and accuracy of the far-field predictions while maintaining the learnability of boundary quantities.

5. Comparison of NCS-BEMNET with other methods

In this section, the performance of NCS-BEMNet is compared with that of the BINN, which is also based on the Boundary Element Method. The comparison focuses on the differences in accuracy and training

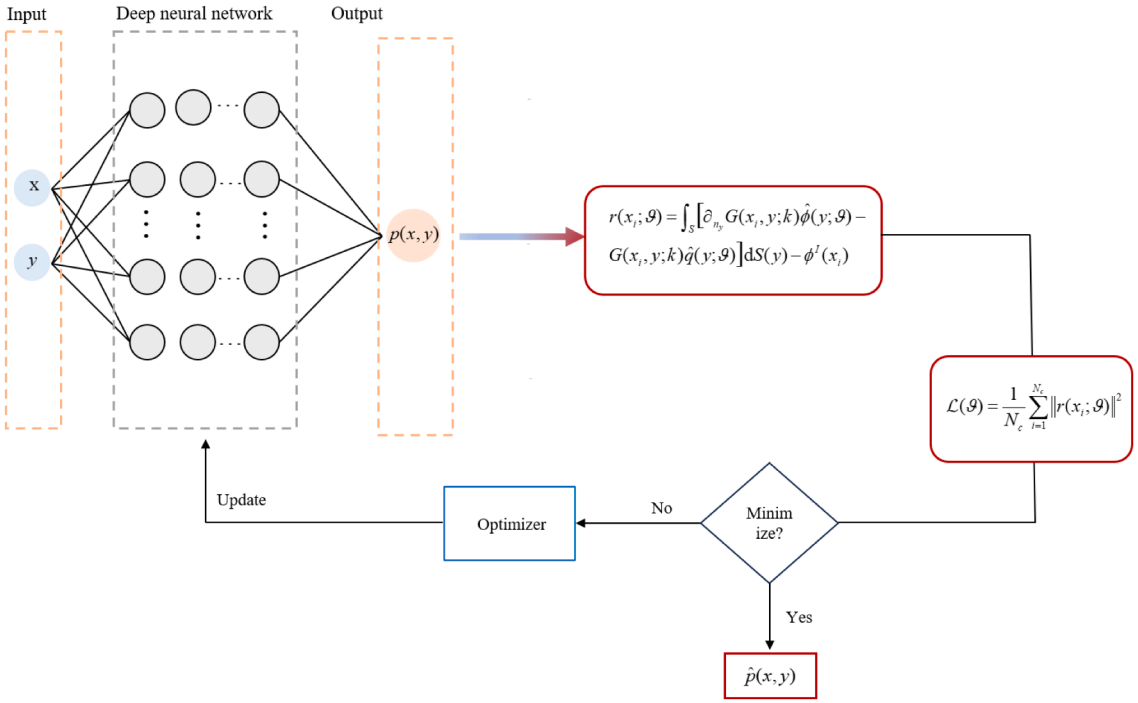

Fig. 9. Framework of the baseline BINN approach used for comparison. The neural network takes the spatial coordinates (x,y) as input and outputs the approximate boundary field $p(x,y)$. The boundary integral equation residual is computed by applying the boundary integral operator, and the network parameters are trained by minimizing the mean squared residual evaluated at boundary collocation points.

efficiency. The main distinction between BINN and NCS-BEMNet lies in the network architecture and input representation, while the loss formulation remains identical. BINN employs a fully connected neural network that takes the boundary point coordinates as input and directly outputs the scattered acoustic pressure on the boundary, representing an explicit spatial mapping approach. In contrast, NCS-BEMNet integrates analytical solution forms and mathematical completeness, reconstructing the acoustic field indirectly through neural coefficients. For a fair comparison, both models are configured with the same number of neural layers and neurons per layer. To facilitate comparison with the proposed NCS-BEMNet, the framework of a BINN approach is illustrated in Fig. 9.

The first benchmark example is a three-dimensional spherical scattering problem, as illustrated in Fig. 10(a). The results show that for this relatively simple 3D acoustic case, both BINN and NCS-BEMNet achieve stable convergence and satisfactory prediction accuracy. However, since the input of BINN consists of boundary point coordinates, its network outputs are initially more dispersed. Consequently, during the first 500 epochs, the loss value of BINN is lower than that of NCS-BEMNet, but its overall convergence is slower. As training proceeds, the prediction accuracy of both models reaches the order of 10^{-4}. Thereafter, the loss of NCS-BEMNet continues to decrease rapidly and eventually converges to approximately 10^{-9}, whereas the loss of BINN saturates around 10^{-6} and shows little further improvement. The final stable accuracy levels of NCS-BEMNet and BINN are approximately 10^{-8} and 10^{-5}, respectively. The corresponding training times are 28.25 s and 24.35 s, indicating that for this simple configuration, the difference in computational cost between the two methods is relatively small.

The second benchmark example concerns a large-scale sonar scattering problem. It can be observed that when the number of boundary points is large, the initial loss values of both methods are similar. This is an occasional phenomenon for NCS-BEMNet, as its input consists of global parameters that can take arbitrary values, leading to random initialization of the loss. For complex acoustic fields, when the BINN network fails to capture fine details, it tends to converge rapidly to a smoothed average representation of the physical field. Although this smooth solution appears stable, it may deviate significantly from the true field distribution. The apparent early convergence gives a misleading impression of successful training, while the network has, in fact, lost the ability to learn the true complex patterns, causing the loss to stagnate.

The training times for NCS-BEMNet and BINN are 11.25 min and 66.55 min, respectively, indicating a clear efficiency advantage of NCS-BEMNet. This difference arises from the distinct network architectures. NCS-BEMNet takes only two global constants, the wavenumber k and the incidence angle, as input, learning a mesh-independent physical mapping. In contrast, BINN requires the coordinates of approximately ten thousand boundary nodes to be input at each iteration, making its learning process strongly coupled with the spatial discretization. As the problem complexity and number of boundary points increase, the input dimensionality of BINN grows linearly, and the computational cost escalates rapidly. NCS-BEMNet, by contrast, demonstrates excellent scalability under these conditions.

To further assess the computational efficiency of the proposed method, a quantitative comparison of training time between NCS-BEMNet and BINN is conducted for acoustic scattering problems with increasing geometric complexity and boundary size. The results are summarized in Table 4. For relatively simple configurations, such as the circular and spherical scattering problems, both methods exhibit comparable computational cost. However, as the number of boundary nodes increases and the geometry becomes more complex, the computational advantage of NCS-BEMNet becomes increasingly pronounced. In particular, for the propeller and sonar scattering problems involving nearly ten thousand boundary nodes, NCS-BEMNet achieves a substantial reduction in training time compared to BINN.

This improvement originates from the mesh-independent architecture of NCS-BEMNet, which learns a global physical mapping using a small number of problem parameters, whereas BINN relies on boundary-point-wise inputs whose dimensionality grows linearly with the boundary discretization. As a result, NCS-BEMNet demonstrates superior scalability for large-scale and engineering-relevant acoustic problems.

Direct wall-clock time comparisons with traditional BEM or FastBEM implementations are not entirely fair, as these methods are typically developed on different computational platforms, programming languages, and solver infrastructures. In particular, classical BEM and FastBEM are often implemented in highly optimized numerical libraries, whereas neural-network-based methods rely on automatic differentiation frameworks and optimization routines that introduce additional overhead. Therefore, instead of relying solely on runtime comparisons, a complexity-based analysis is conducted to provide a more platform-independent perspective, as shown in Table 5.

From a theoretical standpoint, traditional BEM requires the assembly and solution of dense system matrices, resulting in computational costs

Table 4
Computational time comparison between BINN and NCS-BEMNet.

Example	Nodes	BINN Time	NCS-BEMNet Time
Circle	200	10.00 s	6.45 s
Sphere	1200	28.25 s	24.35 s
Propeller	8956	23.15 min	5.44 min
Sonar	12,788	66.55 min	11.25 min

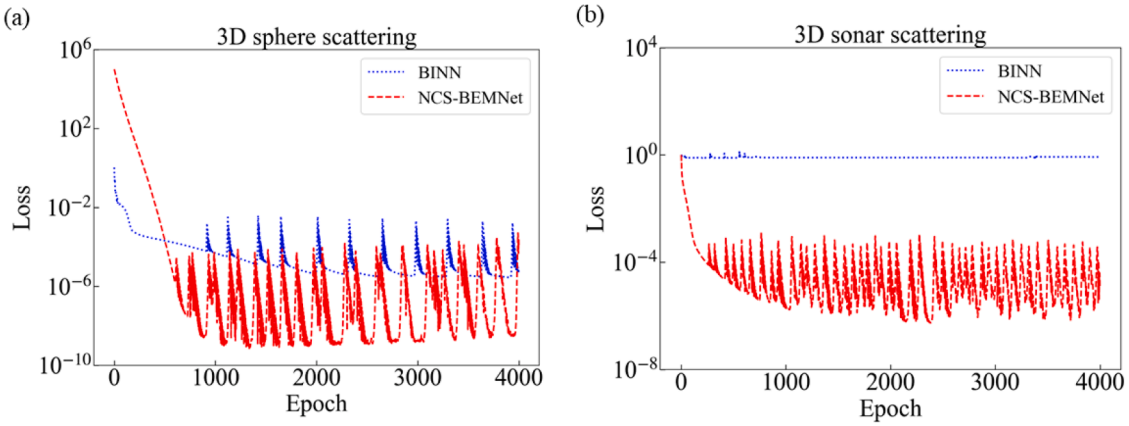

Fig. 10. Comparison of NCS-BEMNet and BINN in three-dimensional acoustic scattering problems. (a) Loss curves for the 3D spherical scattering case with 1200 boundary points. (b) Loss curves for the 3D large-scale sonar scattering case with 12,778 boundary points.

that scale as $O(N_b^3)$ for direct solvers or $O(N_{\text{iter}} \cdot N_b^2)$ for iterative methods. FastBEM techniques alleviate this burden through hierarchical approximations, reducing the dominant complexity to approximately $O(N_b \log N_b)$, but at the expense of increased algorithmic complexity and implementation effort. BINN avoids explicit matrix inversion but still requires global residual evaluations over boundary collocation points $O(T \cdot N_b^2)$, where T denotes the number of optimization steps.

In contrast, the proposed NCS-BEMNet framework replaces dense matrix assembly with projections onto a set of analytical plane-wave bases. The dominant computational cost arises from evaluating boundary integrals and updating expansion coefficients, resulting in an approximate complexity of $O(T \cdot M \cdot nk)$, where $M$is the number of basis functions and d is the spatial dimension. Since $M$is typically much smaller than N_b for practical problems, this structure leads to favorable scaling behavior for large-scale applications. Moreover, the memory requirement grows linearly with the number of boundary nodes and basis functions, avoiding the quadratic storage burden of dense BEM matrices.

Overall, while each method has distinct advantages depending on problem scale and implementation environment, this comparison indicates that NCS-BEMNet provides a balanced trade-off between computational efficiency and solution interpretability.

6. Discussion

Despite the demonstrated accuracy and efficiency of the proposed NCS-BEMNet framework, several limitations should be acknowledged. For clarity, these limitations can be broadly categorized into three aspects: challenges associated with concave geometries, high-frequency scattering regimes, and large-scale computational requirements.

First, for geometries with strong concavities, such as hollow or highly folded structures, the main difficulty does not originate from the neural coefficient solver itself, but rather from the increased complexity of boundary integral kernel interactions. Strong multiple scattering effects and near-singular interactions between closely spaced boundary segments significantly increase the stiffness of the boundary integral residual. While the present implementation remains stable for moderately complex geometries, addressing strongly concave configurations may require advanced strategies.

Second, in high-frequency scattering regimes, where the acoustic wavelength becomes much smaller than the characteristic geometric scale, the surface field exhibits rapid spatial oscillations and strong interference patterns. Accurately capturing such behavior requires a substantially larger number of basis functions to resolve the associated phase variations. As a result, the solution no longer appears smooth in a classical sense, which is a physically expected feature rather than a numerical artifact. The proposed framework requires further improvements in spectral adaptivity and frequency representation to address high-frequency problems.

Third, for large-scale problems with a high number of degrees of freedom, the primary limitation is computational rather than methodological. As the boundary resolution is refined or the frequency increases, the number of plane-wave basis functions required for accurate representation grows accordingly. This leads to imposes substantial demands on GPU computational resources. In the current implementation, large-scale simulations may exceed the available GPU memory, particularly on single-GPU systems with limited capacity.

These limitations naturally point to several promising directions for future research. In particular, adaptive and localized spectral enrichment strategies could be developed to selectively increase the number of basis functions only in regions with strong field variations, while maintaining lower spectral resolution elsewhere. Such approaches are expected to substantially improve GPU utilization efficiency without sacrificing accuracy. In addition, further acceleration techniques, including multi-GPU parallelization, mixed-precision training, and hybridization with classical fast algorithms such as the fast multipole method, offer clear pathways toward extending NCS-BEMNet to ultra-large-scale and high-frequency wave scattering problems.

Overall, the limitations discussed above reflect the inherent trade-offs associated with global analytical approximations and large-scale integral formulations. They do not diminish the effectiveness of the proposed framework, rather, they delineate the current scope of applicability and highlight clear opportunities for future optimization and extension to even more challenging wave-based engineering applications.

Table 5
Comparison of dominant time complexity for BEM, FastBEM, BINN, and NCS-BEMNet.

Complexity Type	BEM	Fast BEM	BINN	NCS-BEMNet
Dominant Time Complexity	$O(N_b^3)$	$O(N_b \log N_b)$	$O(T \cdot (N_b^2))$	$O(T \cdot M \cdot nk)$
Solution Representation	Discrete values	Discrete values	Implicit neural network	Global analytical expansion

7. Conclusion

This study proposes and verifies a neural framework NCS-BEMNet, termed the Neural Coefficient Solver based on the Boundary Element Method, for efficient and accurate solutions of acoustic scattering problems. Numerical results demonstrate that NCS-BEMNet exhibits significantly faster convergence and higher prediction accuracy compared with existing BINN-based approaches. For both simple and complex three-dimensional scattering cases, NCS-BEMNet achieves stable convergence toward lower loss levels, indicating excellent robustness and generalization capability. Unlike the conventional Boundary Element Method, NCS-BEMNet outputs a continuous analytical representation of the acoustic field, effectively overcoming the smoothness assumptions imposed on the boundary in classical formulations and yielding numerically stable, physically consistent solutions. Moreover, its inputs depend only on the global physical parameters of the problem rather than on discretized boundary coordinates. This property substantially reduces training time and computational cost, allowing the model to maintain strong scalability as the problem size increases. The core innovation of NCS-BEMNet lies in the integration of the analytical structure of governing equations with the mathematical completeness of the basis functions. By employing a neural network to learn and refine the expansion coefficients of plane-wave bases within the boundary element formulation, NCS-BEMNet realizes physics-consistent modeling through analytical representation. This structured design enhances model stability and generalization while enabling efficient treatment of acoustic problems involving complex geometries. In summary, NCS-BEMNet provides a novel, practical, and theoretically grounded paradigm for overcoming the accuracy and efficiency limitations inherent in both conventional numerical methods and input-based neural networks for acoustic simulation. The proposed framework demonstrates considerable theoretical and engineering potential for addressing problems in engineering acoustics and related wave physics.

CRediT authorship contribution statement

Huilan Wu: Writing – review & editing, Writing – original draft, Visualization, Software, Methodology, Formal analysis, Data curation. **Yijun Liu:** Project administration, Funding acquisition, Formal analysis, Conceptualization.

Declaration of competing interest

The authors declare that they have no known competing financial interests or personal relationships that could have appeared to influence

the work reported in this paper.

Acknowledgments

The work reported in this article was supported by the National Natural Science Foundation of China (Grant No 12372198).

Supplementary materials

Supplementary material associated with this article can be found, in the online version, at doi:10.1016/j.ijmecsci.2026.111403.

Data availability

The data that support the findings of this study are available from the corresponding authors upon reasonable request.

References

[1] Flax L, Dragonette LR, Überall H. Theory of elastic resonance excitation by sound scattering. J Acoust Soc Am 1978;63(3):723–31.
[2] Sharma GS, et al. Sound scattering by a bubble metasurface. Phys Rev B 2020;102 (21):214308.
[3] Chen Q, et al. Full manipulation of sound scattering via piezoelectric reconfigurable acoustic metamaterials. Phys Rev Appl 2025;23(4):044031.
[4] Liu Y. Fast multipole boundary element method: theory and applications in engineering. Cambridge: Cambridge University Press; 2009.
[5] Harari I. A survey of finite element methods for time-harmonic acoustics. Comput Methods Appl Mech Eng 2006;195(13):1594–607.
[6] Li Y, et al. Efficient dataset generation for inverse design of micro-perforated sonic crystals. Int J Mech Sci 2025;293:110190.
[7] Huttunen T, Kaipio JP, Monk P. An ultra-weak method for acoustic fluid–solid interaction. J Comput Appl Math 2008;213(1):166–85.
[8] Petris G, Cianferra M, Armenio V. A numerical method for the solution of the three-dimensional acoustic wave equation in a marine environment considering complex sources. Ocean Eng 2022;256:111459.
[9] Xi Q, et al. An efficient hybrid collocation scheme for vibro-acoustic analysis of the underwater functionally graded structures in the shallow ocean. Comput Methods Appl Mech Eng 2024;418:116537.
[10] Gui Q, et al. Analysis of two-dimensional acoustic radiation problems using the finite element with cover functions. Appl Acoust 2022;185:108408.
[11] Jansari C, et al. Adaptive enriched geometry independent field approximation for 2D time-harmonic acoustics. Comput Struct 2022;263:106728.
[12] Xie X, et al. Fast model order reduction boundary element method for large-scale acoustic systems involving surface impedance. Comput Methods Appl Mech Eng 2022;400:115618.
[13] Chen L, et al. Broadband topology optimization of three-dimensional structural-acoustic interaction with reduced order isogeometric FEM/BEM. J Comput Phys 2024;509:113051.
[14] Cai Y, et al. Model order reduction of time-domain acoustic finite element simulations with perfectly matched layers. Comput Methods Appl Mech Eng 2024; 431:117298.
[15] Yao L, et al. An optimized finite element method for the analysis of 3D acoustic cavities with impedance boundary conditions. Appl Math Model 2020;84:447–65.
[16] Li H, Thompson D, Squicciarini G. A 2.5D acoustic finite element method applied to railway acoustics. Appl Acoust 2021;182:108270.
[17] van 't Wout E. The boundary element method for acoustic transmission with nonconforming grids. J Comput Appl Math 2024;445:115838.
[18] Castro Mota R, et al. An approximate hybrid approach for computing low-frequency outdoor sound propagation. Eng Anal Bound Elem 2025;179:106308.
[19] Provatidis C, Zafiropoulos N. On the 'interior Helmholtz integral equation formulation' in sound radiation problems. Eng Anal Bound Elem 2002;26(1): 29–40.
[20] Kreuzer W, et al. NumCalc: an open-source BEM code for solving acoustic scattering problems. Eng Anal Bound Elem 2024;161:157–78.
[21] Chen G, Zhou J. Boundary element methods with applications to nonlinear problems, 7. Springer Science & Business Media; 2010.
[22] Harari I, Hughes TJR. A cost comparison of boundary element and finite element methods for problems of time-harmonic acoustics. Comput Methods Appl Mech Eng 1992;97(1):77–102.
[23] Simpson RN, et al. Acoustic isogeometric boundary element analysis. Comput Methods Appl Mech Eng 2014;269:265–90.
[24] Cunefare KA, Koopmann G, Brod K. A boundary element method for acoustic radiation valid for all wavenumbers. J Acoust Soc Am 1989;85(1):39–48.
[25] Jagtap AD, et al. Physics-informed neural networks for inverse problems in supersonic flows. J Comput Phys 2022;466:111402.
[26] Badia S, Li W, Martín AF. Compatible finite element interpolated neural networks. Comput Methods Appl Mech Eng 2025;439:117889.
[27] Raissi M, Perdikaris P, Karniadakis GE. Physics-informed neural networks: a deep learning framework for solving forward and inverse problems involving nonlinear partial differential equations. J Comput Phys 2019;378:686–707.
[28] Jagtap AD, Kawaguchi K, Karniadakis GE. Adaptive activation functions accelerate convergence in deep and physics-informed neural networks. J Comput Phys 2020; 404:109136.
[29] Wang X, et al. Neural network-augmented differentiable finite element method for boundary value problems. Int J Mech Sci 2025;285:109783.
[30] Ye X, et al. On the locality of local neural operator in learning fluid dynamics. Comput Methods Appl Mech Eng 2024;427:117035.
[31] Azizzadenesheli K, et al. Neural operators for accelerating scientific simulations and design. Nat Rev Phys 2024;6(5):320–8.
[32] Cao Q, Goswami S, Karniadakis GE. Laplace neural operator for solving differential equations. Nat Mach Intell 2024;6(6):631–40.
[33] Li R, Ye W, Liu Y. A boundary-based fourier neural operator (B-FNO) method for efficient parametric acoustic wave analysis. Eng Comput 2025;41(4):2393–410.
[34] Li G, et al. Improving generalization ability of deep-learning-based ODE solvers using continuous dependence. npj Artif Intell 2025;1(1):22.
[35] Zhang N, et al. Transfer learning-enhanced finite element-integrated neural networks. Int J Mech Sci 2025;290:110075.
[36] Nagy-Huber M, Roth V. Physics-informed boundary integral networks (PIBI-Nets): a data-driven approach for solving partial differential equations. J Comput Sci 2024;81:102355.
[37] Sun J, et al. A data-driven multi-flaw detection strategy based on deep learning and boundary element method. Comput Mech 2023;71(3):517–42.
[38] Yang L, et al. A hybrid model and data driven approach for ballistic prediction with PINN. Eng Appl Artif Intell 2026;163:112965.
[39] Pratama DA, et al. Solving partial differential equations with hybridized physic-informed neural network and optimization approach: incorporating genetic algorithms and$_L$-BFGS for improved accuracy. Alex Eng J 2023;77:205–26.
[40] Valente M, et al. Physics-consistent machine learning with output projection onto physical manifolds. Commun Phys 2025;8(1):433.
[41] Shin, Y., J. Darbon, and G.E. Karniadakis, *On the convergence of physics informed neural networks for linear second-order elliptic and parabolic type PDEs.* arXiv preprint arXiv:2004.01806, 2020.
[42] He J, Tiamiyu AT. Physics-informed neural networks in iterative form of nonlinear equations for numerical algorithms and simulations of delay differential equations. Phys A: Stat Mech Appl 2025;660:130368.
[43] Ambrosio P, Cuomo S, De Rosa M. A physics-informed deep learning approach for solving strongly degenerate parabolic problems. Eng Comput 2024:1–17.
[44] Zhang F, Nghiem L, Chen Z. A novel approach to solve hyperbolic Buckley-Leverett equation by using a transformer based physics informed neural network. Geoenergy Sci Eng 2024;236:212711.
[45] Zhou J, Li R, Luo T. Physics-informed neural networks for solving time-dependent mode-resolved phonon Boltzmann transport equation. npj Comput Mater 2023;9 (1):212.
[46] Liu X-Y, et al. Multi-resolution partial differential equations preserved learning framework for spatiotemporal dynamics. Commun Phys 2024;7(1):31.
[47] Meng X, et al. PPINN: parareal physics-informed neural network for time-dependent PDEs. Comput Methods Appl Mech Eng 2020;370:113250.
[48] Wu Y, et al. Randomized radial basis function neural network for solving multiscale elliptic equations. Mach Learn: Sci Technol 2025;6(1):015033.
[49] Wang Y, et al. A practical PINN framework for multi-scale problems with multi-magnitude loss terms. J Comput Phys 2024;510:113112.
[50] Ouyang C, et al. Physics-infused KAN for turbulent flow prediction and CFD integration. Int J Mech Sci 2026;311:111185.
[51] Toscano JD, et al. AIVT: inference of turbulent thermal convection from measured 3D velocity data by physics-informed Kolmogorov-Arnold networks. Sci Adv 2025; 11(19):eads5236.
[52] Zhang E, et al. Analyses of internal structures and defects in materials using physics-informed neural networks. Sci Adv 2022;8(7):eabk0644.
[53] He W, et al. Multi-level physics informed deep learning for solving partial differential equations in computational structural mechanics. Commun Eng 2024;3 (1):151.
[54] Sun H, et al. Physics-informed neural network for velocity prediction in electromagnetic launching manufacturing. Mech Syst Signal Process 2024;220: 111671.
[55] Su Y, et al. Physics-informed graph neural network for electromagnetic simulations. In: 2023 XXXVth General Assembly and Scientific Symposium of the International Union of Radio Science (URSI GASS). IEEE; 2023.
[56] Lee SY, et al. A physics-informed and data-driven deep learning approach for wave propagation and its scattering characteristics. Eng Comput 2023;39(4):2609–25.
[57] Borate P, et al. Using a physics-informed neural network and fault zone acoustic monitoring to predict lab earthquakes. Nat Commun 2023;14(1):3693.
[58] Liu C-X, et al. A physics-informed neural network for Kresling origami structures. Int J Mech Sci 2024;269:109080.
[59] Pun GPP, et al. Physically informed artificial neural networks for atomistic modeling of materials. Nat Commun 2019;10(1):2339.
[60] Tarancón-Álvarez P, et al. Efficient PINNs via multi-head unimodular regularization of the solutions space. Commun Phys 2025;8(1):335.
[61] Movahhedi M, et al. Predicting 3D soft tissue dynamics from 2D imaging using physics informed neural networks. Commun Biol 2023;6(1):541.
[62] Piao S, et al. A domain-adaptive physics-informed neural network for inverse problems of Maxwell's equations in heterogeneous Media. IEEE Antennas Wirel Propag Lett 2024;23(10):2905–9.

[63] Yuan L, et al. A-PINN: auxiliary physics informed neural networks for forward and inverse problems of nonlinear integro-differential equations. J Comput Phys 2022;462:111260.
[64] Liu C, Wu H. cv-PINN: efficient learning of variational physics-informed neural network with domain decomposition. Extreme Mech Lett 2023;63:102051.
[65] Jagtap AD, Karniadakis GE. Extended physics-informed neural networks (XPINNs): a generalized space-time domain decomposition based deep learning framework for nonlinear partial differential equations. Commun Comput Phys 2020;(5):28.
[66] Gu L, et al. Physics-informed neural networks with domain decomposition for the incompressible Navier–Stokes equations. Phys Fluids 2024;36(2).
[67] Duan J, Zhao H, Song J. Spatial domain decomposition-based physics-informed neural networks for practical acoustic propagation estimation under ocean dynamics. J Acoust Soc Am 2024;155(5):3306–21.
[68] Zhang B, et al. Multi-domain physics-informed neural network for solving forward and inverse problems of steady-state heat conduction in multilayer media. Phys Fluids 2022;34(11).
[69] Escapil-Inchauspé P, Ruz GA. Hyper-parameter tuning of physics-informed neural networks: application to Helmholtz problems. Neurocomputing 2023;561:126826.
[70] Schmid JD, et al. Physics-informed neural networks for acoustic boundary admittance estimation. Mech Syst Signal Process 2024;215:111405.
[71] Cheng R, Yin X, Chen L. Machine Learning enhanced boundary ElementMethod: prediction of gaussian quadrature points. CMES-Comput Model Eng Sci 2022;131(1).
[72] Li Y, et al. A general-purpose machine learning framework for predicting singular integrals in boundary element method. Eng Anal Bound Elem 2020;117:41–56.
[73] Huang S, et al. Machine learning to approximate free-surface Green's function and its application in wave-body interactions. Eng Anal Bound Elem 2022;134:35–48.
[74] Yuan X, et al. Acoustic sensitivity analysis considering ground reflection using Bayesian neural network-accelerated isogeometric boundary element method. Eng Comput 2026;42(1):26.
[75] Qiu W, Chen H, Zhou H. Real-time identification of temperature-dependent thermo-mechanical properties of specific pressure vessels via deep learning. Eng Anal Bound Elem 2025;180:106514.
[76] Zhou W, Yang X, Chen Y. Adaptive sinh transformation gaussian quadrature for 2D potential problems using deep learning. Eng Anal Bound Elem 2023;155:197–211.
[77] Ma H, Zou C. Boundary learning neural network for efficient solution of elliptic PDEs via boundary integral equations. Eng Anal Bound Elem 2025;180:106503.
[78] Sun J, et al. BINN: a deep learning approach for computational mechanics problems based on boundary integral equations. Comput Methods Appl Mech Eng 2023;410:116012.
[79] Zhang P, et al. Boundary integrated neural networks for 2D elastostatic and piezoelectric problems. Int J Mech Sci 2024;280:109525.
[80] Qu W, et al. Boundary integrated neural networks and code for acoustic radiation and scattering. Int J Mech Syst Dyn 2024;4(2):131–41.
[81] Ruocco E, Fusco P, Musone V. An efficient Artificial Neural Network algorithm for solving boundary integral equations in elasticity. Eng Anal Bound Elem 2023;156:379–91.
[82] Shen W, et al. A rasterized plane wave expansion method for complex 2-D phononic crystals. Mech Syst Signal Process 2024;212:111324.
[83] Meixner J. Die Greensche funktion der Diracgleichung. Ann Phys 1937;421(2):97–116.
[84] Weyl H. Ausbreitung elektromagnetischer Wellen über einem ebenen leiter. Ann Phys 1919;365(21):481–500.
[85] Pierce AD. Acoustics: an introduction to its physical principles and applications. Springer International Publishing; 2019.
[86] Felsen LB, Marcuvitz N. Radiation and scattering of waves. Wiley; 1994.
[87] Cheng AHD, Chen CS, Karageorghis A. An introduction to the method of fundamental solutions. World Scientific; 2024. p. 616.
[88] Liu Z, et al. The method of fundamental solutions for the elastic wave scattering in a double-porosity dual-permeability medium. Appl Math Model 2021;97:721–40.